Supporting information for:

Post-polymerization functionalization of poly(ethylene oxide)-poly(β-6-heptenolactone) diblock copolymers to tune properties and self-assembly

Brooke M. Raycraft,[a] *Jarret P. MacDonald,*[a,b] *James T. McIntosh,*[a] *Michael P. Shaver,*[b] *and Elizabeth R. Gillies*[a,c*]

[a]Department of Chemistry and Center for Advanced Materials and Biomaterials Research (CAMBR), The University of Western Ontario, 1151 Richmond St., London, Canada N6A 5B7

[b]School of Chemistry, University of Edinburgh, Joseph Black Building, David Brewster Road, Edinburgh, EH9 3FJ

[c]Department of Chemical and Biochemical Engineering, The University of Western Ontario, 1151 Richmond St., London, Canada N6A 5B9

Table of contents

General materials and procedures as well as some representative procedures can be found in the main manuscript

Synthesis of PEO_{45}-*b*-$PHEL_{45}$. This polymer was synthesized as described for PEO_{45}-*b*-$PHEL_{23}$ except that the following quantities were used: β-6-HEL (2.00 g, 15.9 mmol, 51 equiv.), [Al] (170 mg, 0.31 mmol, 1.0 equiv.), PEO (620 mg, 0.31 mmol, 1.0 equiv.), toluene (20 mL). Yield = 90%. ^{1}H NMR (600 MHz, $CDCl_3$): δ 1.69 – 1.71 (m, 92H), 2.04 – 2.07 (m, 97H), 2.47 – 2.62 (m, 92H), 3.38 (s, 3H), 3.64 (br s, 180H), 4.20 – 4.22 (m, 2H), 4.96 – 5.04 (m, 93H), 5.20-5.23 (m, 45H), 5.72-5.82 (m, 45H). M_n based on ^{1}H NMR spectroscopy = 7040 g mol^{-1}. SEC (THF): M_n = 6630 g mol^{-1}, M_w = 7860 g mol^{-1}, $Đ$ = 1.19. FTIR: 2863, 1736, 1641 cm^{-1}. T_m = 29˚C. T_g = -59˚C.

Synthesis of PEO_{45}-*b*-$PHEL_{79}$. This polymer was synthesized as described for PEO_{45}-*b*-$PHEL_{23}$ except that the following quantities were used: β-6-HEL (2.20 g, 17.4 mmol, 92 equiv.), [Al] (106 mg, 0.19 mmol, 1.0 equiv.), PEO (387 mg, 0.19 mmol, 1.0 equiv.), toluene (15 mL). Yield = 83%. ^{1}H NMR (600 MHz, $CDCl_3$): δ 1.68 – 1.71 (m, 171H), 2.04 – 2.09 (m, 170H), 2.48 – 2.61 (m, 173H), 3.38 (s, 3H), 3.64 (br s, 180H), 4.20 – 4.23 (m, 2H), 4.97 – 5.03 (m, 158H), 5.21-5.22 (m, 81H), 5.74 – 5.80 (m, 76H). M_n based on ^{1}H NMR spectroscopy = 10848 g mol^{-1}. SEC (THF): M_n = 12910 g mol^{-1}, M_w = 13340 g mol^{-1}, $Đ$ = 1.03. FTIR: 2924, 1737, 1642 cm^{-1}. T_m = 22˚C. T_g = -46˚C.

Synthesis of PEO_{45}-*b*-$PHEL_{31}$-TEG_{14}. The same procedure as for the synthesis of PEO_{45}-*b*-$PHEL_{21}$-$octyl_{24}$ was used except that the following reagents and quantities were used. Polymer =

PEO_{45}-*b*-$PHEL_{45}$ (50.0 mg, 6.0 μmol); thiol = TEG-thiol (27.0 mg, 0.150 mmol); initiator = DMPA (1.92 mg, 8.0 μmol); solvent = toluene (1 mL). The polymer was purified by dialysis using 3500 MWCO regenerated cellulose membrane in DMF. Yield = 74%. ^{1}H NMR (600 MHz, $CDCl_3$): δ 1.39-1.42 (m, 30H), 1.56 – 1.60 (m, 55H), 1.69 – 1.73 (m, 66H), 2.05 – 2.09 (m, 68H), 2.51 – 2.57 (m, 118H), 2.69 (t, 27H, J = 7.0 Hz), 3.37 (s, 45H), 3.54-3.55 (m, 28H), 3.64 (bs, 275H), 4.20 – 4.22 (m, 2H), 4.96 – 5.03 (m, 62H), 5.18 – 5.21 (m, 45H), 5.73 – 5.80 (m, 29H). M_n based on ^{1}H NMR spectroscopy = 10549 g mol^{-1}. SEC (THF): M_n = 7710 g mol^{-1}, M_w = 8840 g mol^{-1}, $Đ$ = 1.15. FTIR: 2865, 1735, 1640. T_m = 29˚C. T_g = -44˚C.

Synthesis of PEO_{45}-*b*-CA_{45}. The same procedure as for the synthesis of PEO_{45}-*b*-$PHEL_{21}$-$octyl_{24}$ was used except that the following reagents and quantities were used. Polymer = PEO_{45}-*b*-$PHEL_{45}$ (500 mg, 0.063 mmol); thiol = thioglycolic acid (936 mg, 8.82 mmol); initiator = DMPA (113 mg, 0.441 mmol); solvent = toluene (4 mL). The polymer was purified by dialysis using 3500 g mol^{-1} MWCO regenerated cellulose membrane in DMF. Yield = 61%. ^{1}H NMR (600 MHz, $CDCl_3$): δ 1.29 – 1.32 (m, 95H), 1.50 – 1.52 (m, 189H), 2.44 – 2.54 (m, 188H), 3.13 (s, 88H), 3.27 (s, 4H), 3.54 (bs, 180H), 4.10 – 4.12 (m, 2H), 5.05 – 5.09 (m, 46H), 11.18 (br s, 41H). M_n based on ^{1}H NMR spectroscopy = 11180 g mol^{-1}. FTIR: 3447, 2940, 2870, 1726, 1640 cm^{-1}. T_g = -19˚C.

Synthesis of PEO_{45}-*b*-$PHEL_{20}$-CA_{25}. The same procedure as for the synthesis of PEO_{45}-*b*-$PHEL_{21}$-$octyl_{24}$ was used except that the following reagents and quantities were used. Polymer = PEO_{45}-*b*-$PHEL_{45}$ (250 mg, 0.033 mmol); thiol = thioglycolic acid (62.0 mg, 0.673 mmol); initiator = DMPA (8.7 mg, 0.034 mmol); solvent = toluene (3 mL). The polymer was purified by

dialysis using 3500 g mol^{-1} MWCO regenerated cellulose membrane in DMF. Yield = 58%. ^{1}H NMR (600 MHz, $CDCl_3$): δ 1.37 – 1.45 (m, 49H), 1.49 – 1.75 (m, 138H), 2.03 (m, 44H), 2.40 – 2.68 (m, 133H), 3.19 (m, 42H), 3.42 (s, 3H), 3.60 (br s, 180H), 4.16-4.18 (m, 2H), 4.89 – 5.03 (m, 42H), 5.18-5.22 (m, 44H), 5.66 – 5.79 (m, 20H). M_n based on ^{1}H NMR spectroscopy = 9341 g mol^{-1}. FTIR: 3463, 2933, 2869, 1732, 1644 cm^{-1}. T_g = -46˚C.

Synthesis of PEO_{45}-*b*-CA_{11}-PTX_{34}. In a flame-dried flask equipped with stir bar, PEO_{45}-*b*-CA_{45} (75.0 mg, 0.007 mmol, equiv.) was dissolved in dry DMF (5 mL). Paclitaxel (550 mg, 0.070 mmol, equiv.), EDC·HCl (147 mg, 0.710 mmol, equiv.) and DMAP (33 mg, 0.271 mmol, equiv.) were added and the reaction mixture was stirred overnight. The polymer was precipitated into cold ethanol and purified by dialysis using 6000-8000 g mol^{-1} MWCO membrane in DMF. Yield = 49%. ^{1}H NMR (600 MHz, $CDCl_3$): δ 1.10 – 1.63 (m, 696H), 1.78 – 2.47 (m, 826H), 3.21 – 3.26 (m, 85H), 3.64 (br s, 190H), 3.73 – 3.79 (m, 34H), 4.11 – 4.18 (m, 34H), 4.22 – 4.28 (m, 33H), 4.32 – 4.45 (m, 30H), 4.88 – 4.98 (m, 35H), 5.08 – 5.25 (m, 45H), 5.50 – 5.56 (m, 36H), 5.61 – 5.67 (m, 41H), 5.90 – 5.60 (m, 34H), 6.13 – 6.24 (m, 40H), 6.25 – 6.31 (s, 29H), 7.27 – 7.71 (m, 513H), 8.08 – 8.14 (m, 76H). M_n based on ^{1}H NMR spectroscopy = 39601 g mol^{-1}. SEC (THF): M_n = 9010 g mol^{-1}, M_w = 16920 g mol^{-1}, $Đ$ = 1.88. FTIR: 3447, 2940, 1726. T_g = 131˚C.

Synthesis of PEO_{45}-*b*-$PHEL_{20}$-CA_7-PTX_{18}. This polymer was synthesized as described above for PEO_{45}-*b*-CA_{11}-PTX_{34} except that the following quantities were used: PEO_{45}-*b*-$PHEL_{20}$-CA_{25} (50.0 mg, 0.005 mmol, 1.0 equiv.); paclitaxel (269 mg,0.315 mmol, 63 equiv.); EDC·HCl (66 mg, 0.345 mmol, 69 equiv.); DMAP (17 mg, 0.140 mmol, 28 equiv.); DMF (4 mL). Yield = 56%. ^{1}H NMR (600 MHz, $CDCl_3$): δ 1.10 –1.63 (m, 620H), 1.78 – 2.47 (m, 592H), 3.21 – 3.26

(m, 32H), 3.64 (br s, 180H), 3.73 – 3.79 (m, 18H), 4.11 – 4.18 (m, 19H), 4.22 – 4.28 (m, 16H), 4.32 – 4.45 (m, 17H), 4.88 – 4.98 (m, 59H), 5.08 – 5.25 (m, 44H), 5.50 – 5.56 (m, 18H), 5.61 – 5.67 (m, 45H), 5.90 – 5.60 (m, 16H), 6.13 – 6.24 (m, 17H), 6.25 – 6.31 (br s, 18H), 6.85 – 7.71 (m, 452H), 8.08 – 8.14 (m, 55H). M_n based on ^{1}H NMR spectroscopy = 24387 g mol^{-1}. M_n = 6750 g mol^{-1}, M_w = 8800 g mol^{-1}, $Đ$ = 1.30. FTIR: 3459, 2940, 1726, 1242, 704 cm^{-1}. T_g = 87°C.

Synthesis of anhydride 2. Dicyclohexylcarbodiimide (656 mg, 3.2 mmol, 0.6 equiv.) in dry CH_2Cl_2 (5 mL) was added to a solution of 3-tritylsulfanyl-propionic acid (**1**) (2.0 g, 5.7 mmol, 1.0 equiv.) dissolved in dry CH_2Cl_2 (15 mL). The reaction mixture was stirred at room temperature for 10 h and filtered to remove dicyclohexylurea byproduct. The resulting solution was then concentrated, washed with ethyl acetate and dried under vacuum to give **2** as a white solid. Yield = 86%. ^{1}H NMR (600 MHz, $CDCl_3$): δ 2.25 (4H, t, J = 7.3 Hz), 2.50 (4H, t, J = 7.3 Hz), 7.21 – 7.24 (6H, m), 7.30 (12H, t, J = 7.6 Hz), 7.50 (12H, d, J = 7.6 Hz). ^{13}C NMR (125 MHz, DMSO): δ 167.4, 144.1, 129.1, 128.1, 126.8, 66.3, 33.8, 25.8. FTIR: 3069, 2939, 1819, 1701 cm^{-1}. HRMS calcd for $[M+Na]^+$ $C_{44}H_{38}O_3S_2Na$: 701.2160; found: 701.2160.

Synthesis of rhodamine derivative 4. A solution of rhodamine derivative **3**[1] (500 mg, 1.03 mmol, 1.0 equiv.) in dry THF (14 mL) was added dropwise to a solution of the anhydride **2** (350 mg, 0.516 mmol, 0.5 equiv.) dissolved in dry THF (10 mL). The reaction mixture was stirred overnight at room temperature. The solvent was evaporated and the product was purified by column chromatography using neutral alumina (EtOAc:Hexanes (1:1)). Yield = 36%. ^{1}H NMR (600 MHz, $CDCl_3$, δ): 1.17 (t, 12H J = 7.1 Hz), 2.06 (dd, 3H, J = 9.3, 5.7 Hz), 2.44 (t, 2H, J = 7.5 Hz), 2.98 – 3.03 (m, 2H), 3.27 – 3.38 (m, 10H), 6.24 (dd, 2H, J = 8.9, 2.5 Hz), 6.39 (d, 2H, J = 2.5 Hz), 6.41 (d, 2H, J = 8.9 Hz), 6.66 (t, 1H, J = 4.1 Hz), 7.10 (dd, 1H, J = 6.1, 1.6 Hz), 7.19

(t, 3H, J = 7.3 Hz), 7.41 (d, 6H, J = 7.5 Hz), 7.26 (t, 6H, J = 7.7 Hz), 7.44 – 7.49 (m, 2H), 7.89 (dd, 1H, J = 6.2, 2.0 Hz). ^{13}C NMR (125 MHz, $CDCl_3$): δ 170.85, 169.97, 153.98, 153.36, 149.02, 144.93, 132.86, 130.61, 129.73, 128.61, 128.06, 127.99, 127.95, 126.69, 124.04, 104.86, 97.81, 65.66, 66.71, 44.48, 40.71, 35.99, 27.92, 12.75. FTIR: 3081, 2966, 1721, 1615, 1514 cm^{-1} HRMS calcd for $[M]^+$ $C_{52}H_{54}N_4O_3S$: 814.3917; found: 814.3928.

Synthesis of PEO_{45}-*b*-$PHEL_{40}$-RHD_5. To a solution of rhodamine derivative **4** (215 mg, 0.264 mmol, 1.0 equiv.) dissolved in dry CH_2Cl_2 (1 mL) was added a solution of TFA:CH_2Cl_2 (1:1) (1 mL) dropwise at 0 ˚C. The reaction mixture was stirred at room temperature for 4 hr and monitored by TLC. The solvent was evaporated, and the resulting thiol product was used immediately without further purification. To a 10 mL Schlenk tube equipped with a stir bar, a mixture of PEO_{45}-*b*-$PHEL_{45}$ (50.0 mg, 0.007 mmol, 1.0 equiv.), deprotected **4** (145 mg, 0.253 mmol, 36 equiv.) and azobisisobutyronitrile (AIBN) (8.0 mg, 0.050 mmol, 7.1 equiv.) in toluene (6 mL) were added and degassed by three cycles of freeze pump thaw. The reaction mixture was then stirred at 80 °C for 6 hours. The resulting polymer was purified by dialysis using 6000-8000 g mol^{-1} MWCO membrane in DMF. Yield = 69%. ^{1}H NMR (600 MHz, $CDCl_3$): δ 1.15 (t, 65H, J = 7.0 Hz), 1.71 (br s, 94H), 2.02 – 2.07 (m, 103H), 2.41 (t, 14H, J = 7.3 Hz), 2.50 – 2.58 (m, 94H), 2.95 – 2.96 (m, 11H), 3.25 – 3.32 (m, 51H), 3.64 (br s, 180H), 4.22 (br s, 2H), 4.97 – 5.04 (m, 84H), 5.21 – 5.23 (m, 45H), 5.74 – 5.81 (m, 40H), 6.22 (dd, 9H, J = 8.8, 2.4 Hz), 6.39 (d, 19H, J = 9.4 Hz), 6.62 (br s, 4H), 7.07 (d, 6H, J = 7.0 Hz), 7.15 – 7.18 (m, 14H), 7.24 (t, 28H, J = 7.6 Hz), 7.38 (d, 28H, J = 7.3 Hz), 7.45 (quin, 12H, J = 6.9 Hz), 7.86 (d, 5H, J = 7.0 Hz). M_n based on ^{1}H NMR spectroscopy = 11115 g mol^{-1}. SEC (THF): M_n = 6300 g mol^{-1}, M_w = 7260 g mol^{-1}, $Đ$ = 1.15. FTIR: 3081, 2930, 2866, 1739, 1721, 1640, 1616, 1518 cm^{-1}. T_g = -33 ˚C.

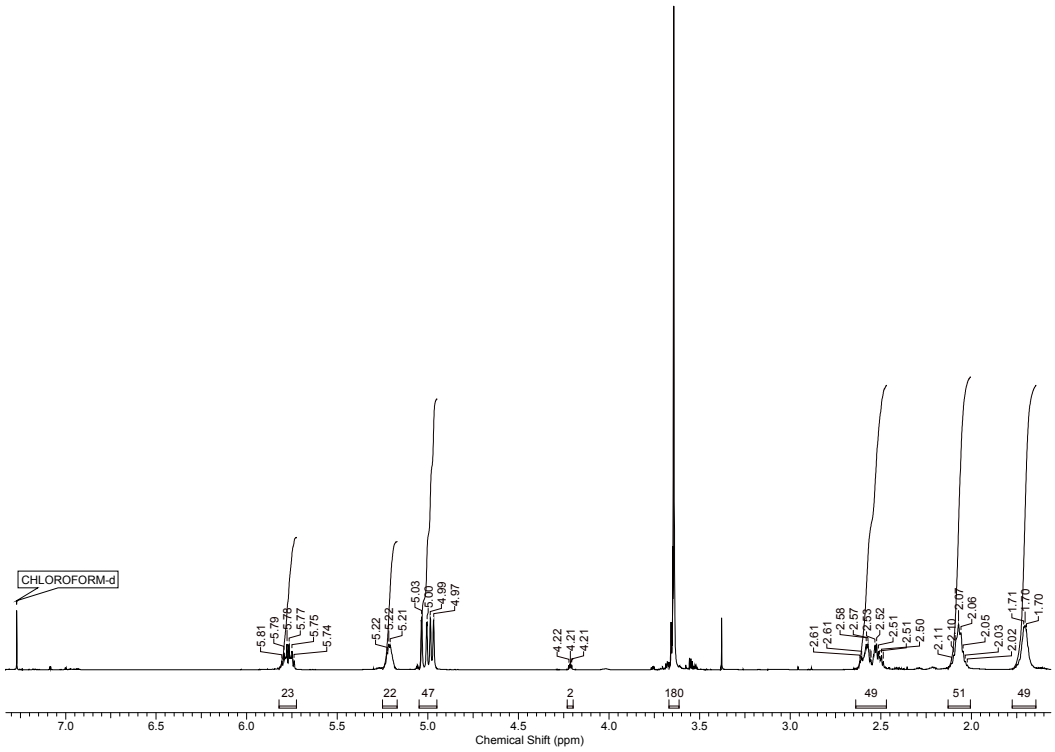

Figure S1. ^{1}H NMR spectrum of PEO_{45}-*b*-$PHEL_{23}$ (600 MHz, $CDCl_3$).

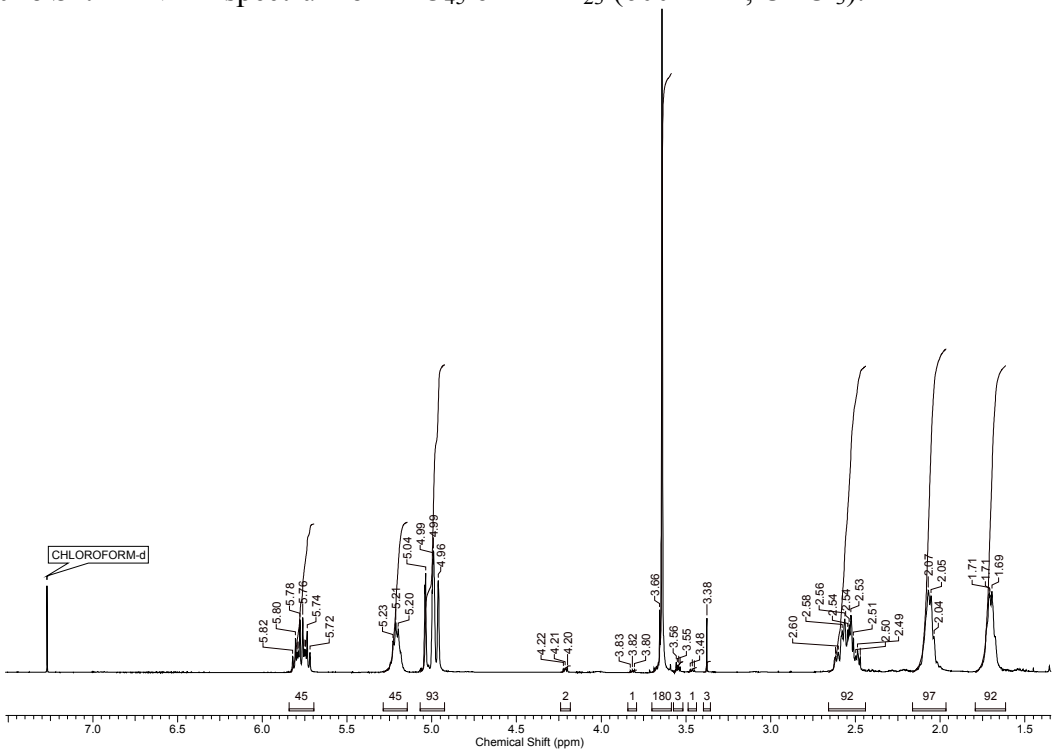

Figure S2. ^{1}H NMR spectrum of PEO_{45}-*b*-$PHEL_{45}$ (600 MHz, $CDCl_3$).

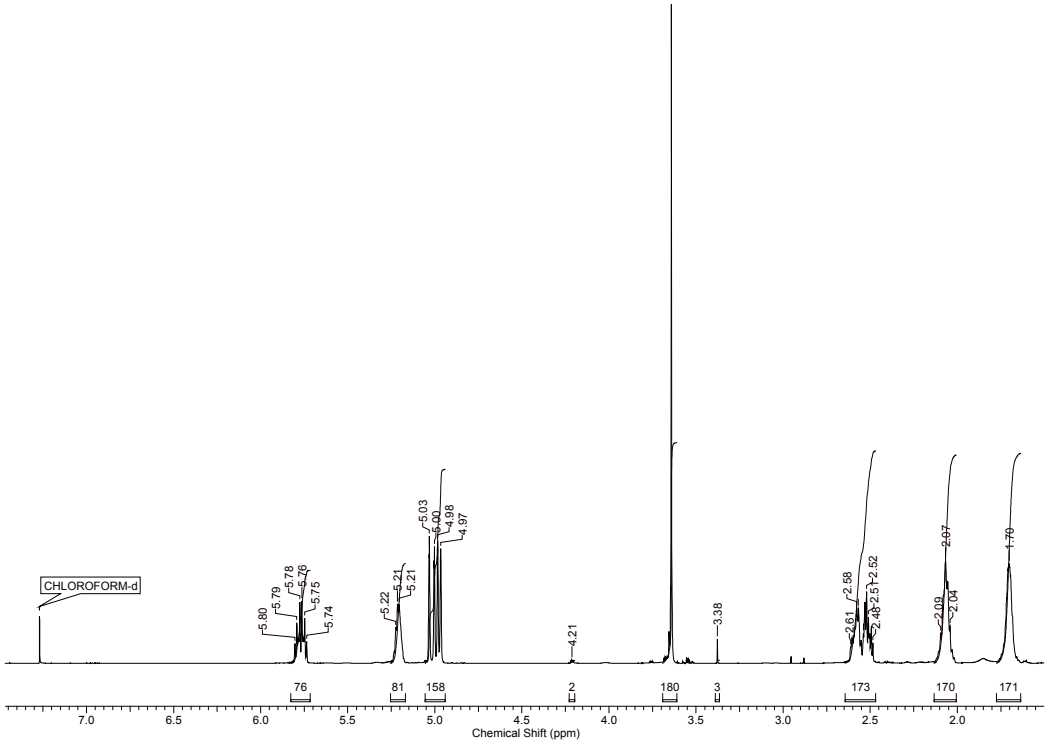

Figure S3. ^{1}H NMR spectrum of PEO_{45}-*b*-$PHEL_{79}$ (600 MHz, $CDCl_3$).

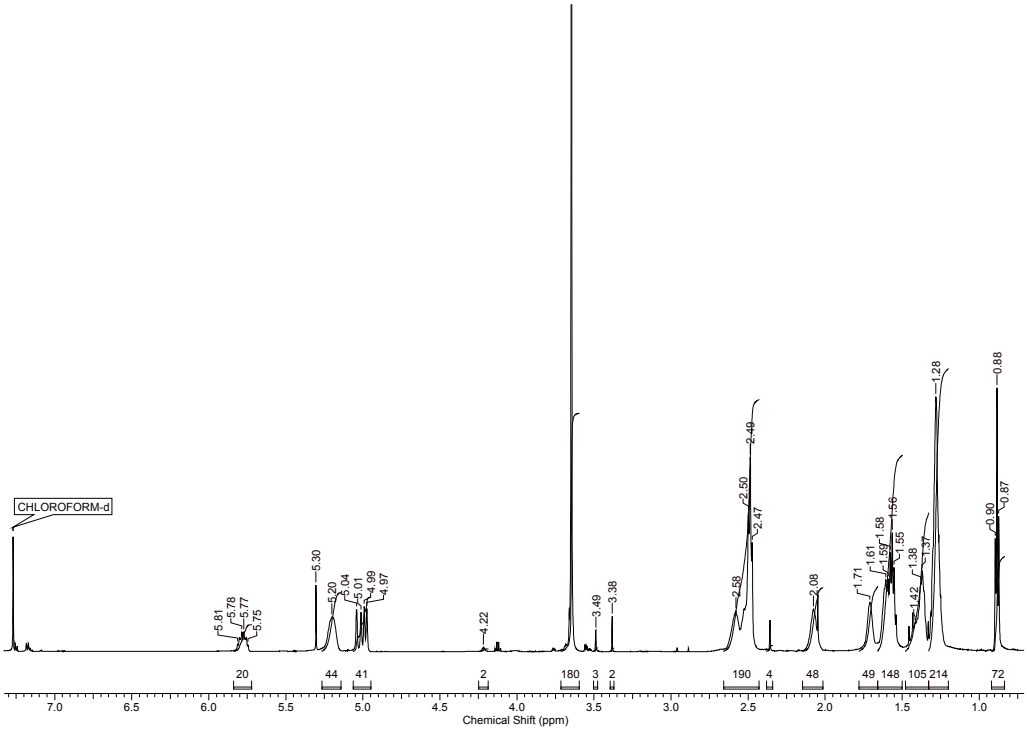

Figure S4. ^{1}H NMR spectrum of PEO_{45}-*b*-$PHEL_{21}$-$octyl_{24}$ (600 MHz, $CDCl_3$).

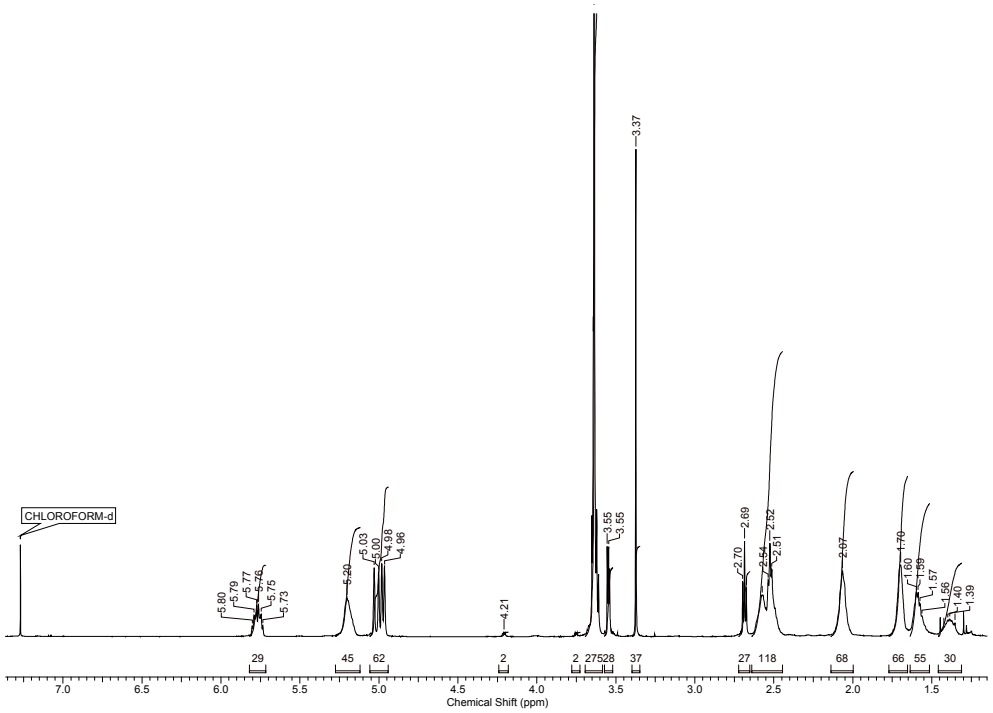

Figure S5. ^{1}H NMR spectrum of PEO_{45}-*b*-$PHEL_{31}$-TEG_{14} (600 MHz, $CDCl_3$).

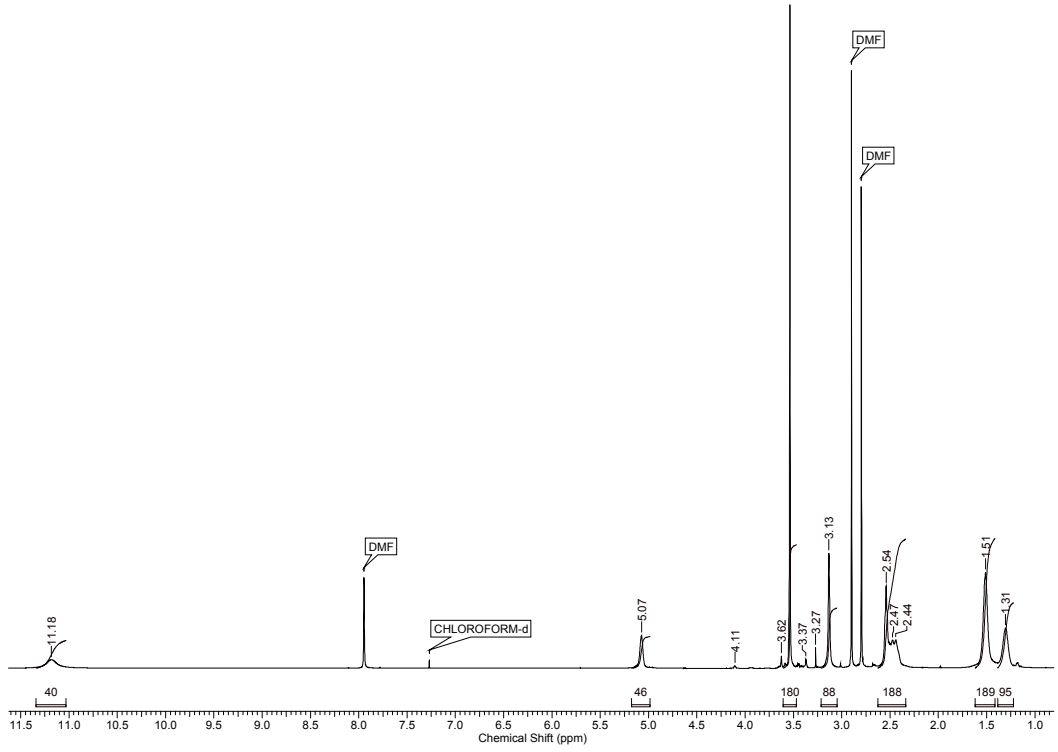

Figure S6. ^{1}H NMR spectrum of PEO_{45}-*b*-CA_{45} (600 MHz, $CDCl_3$).

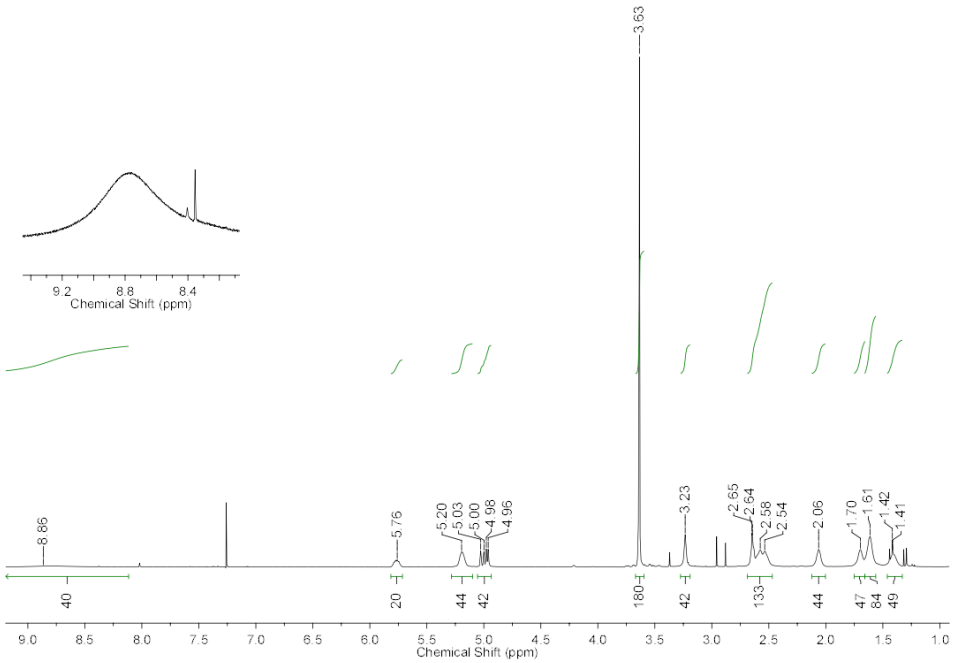

Figure S7. ^{1}H NMR spectrum of PEO_{45}-*b*-$PHEL_{20}$-CA_{25} (600 MHz, $CDCl_3$).

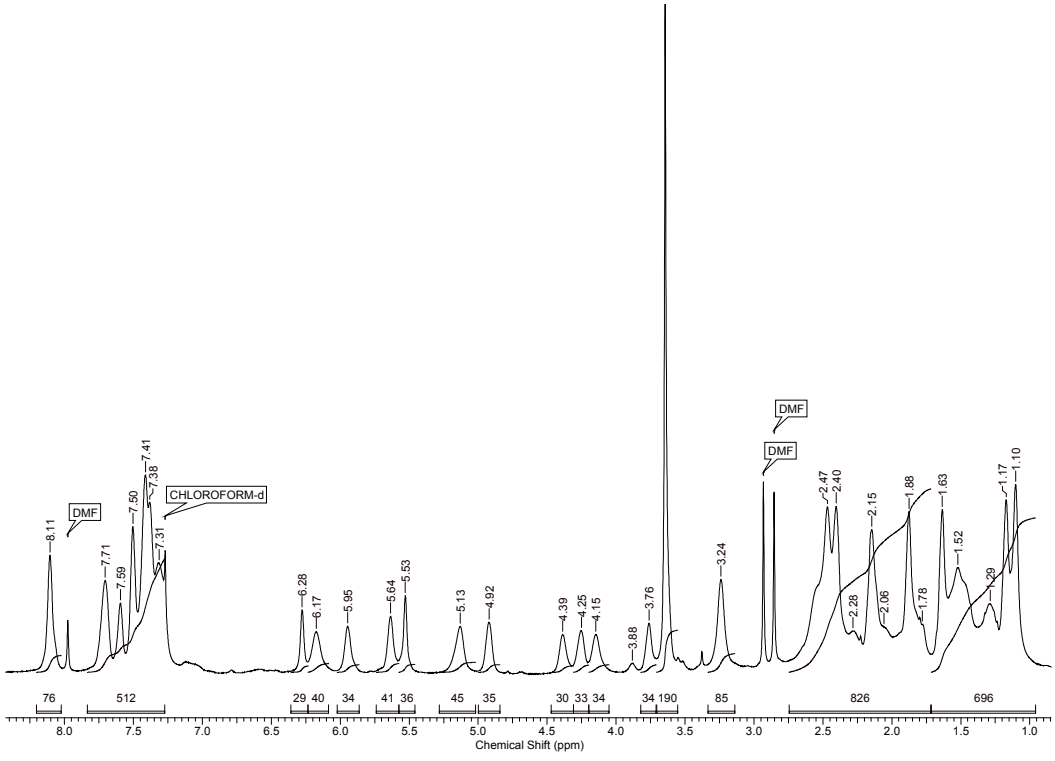

Figure S8. ^{1}H NMR spectrum of PEO_{45}-*b*-CA_{11}-PTX_{34} (600 MHz, $CDCl_3$).

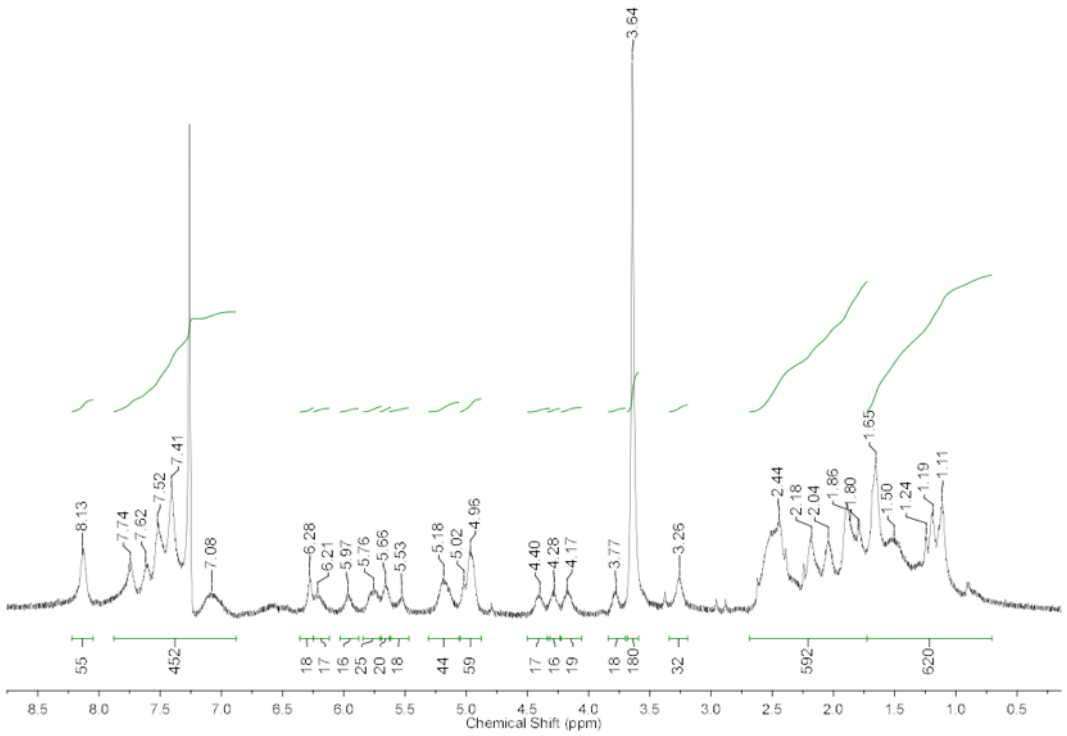

Figure S9. ^{1}H NMR spectrum of PEO_{45}-*b*-$PHEL_{20}$-CA_{7}-PTX_{18} (600 MHz, $CDCl_3$).

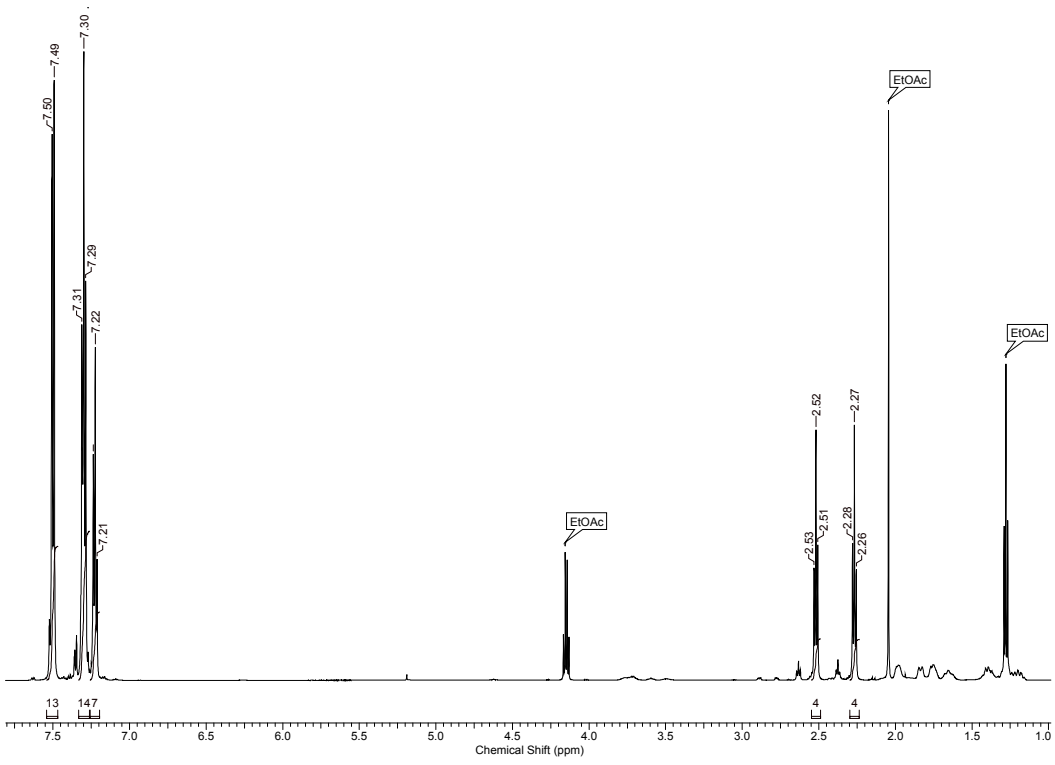

Figure S10. ^{1}H NMR spectrum of **2** (600 MHz, $CDCl_3$).

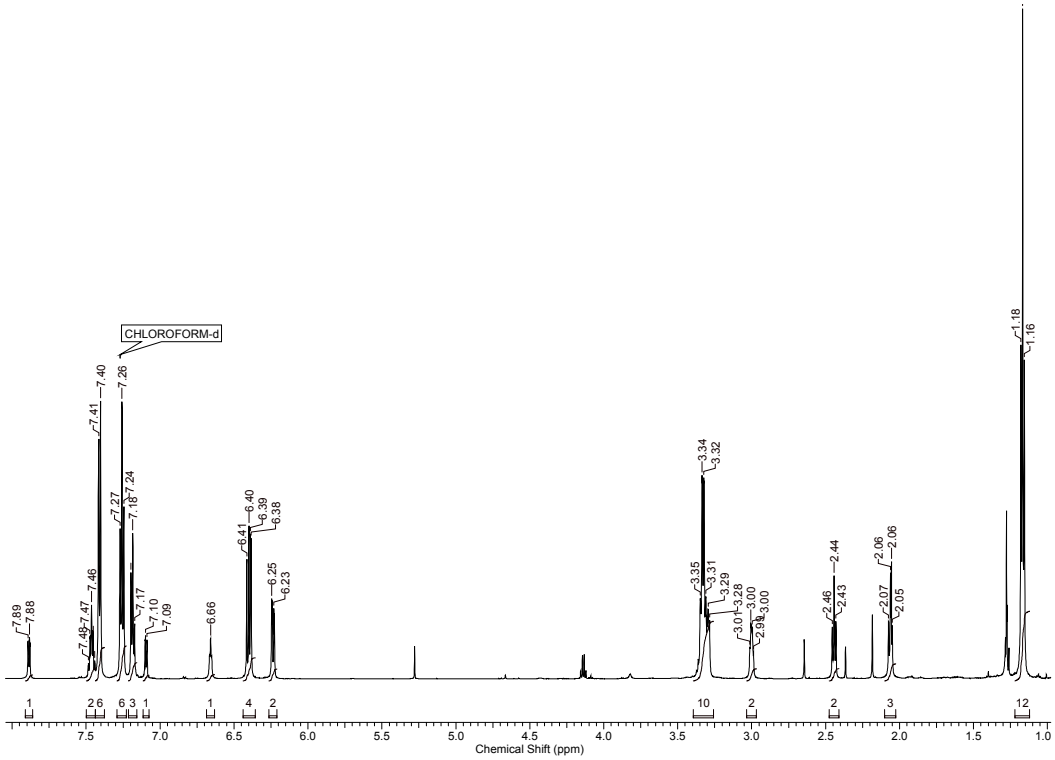

Figure S11. ^{1}H NMR spectrum of **4** (600 MHz, $CDCl_3$).

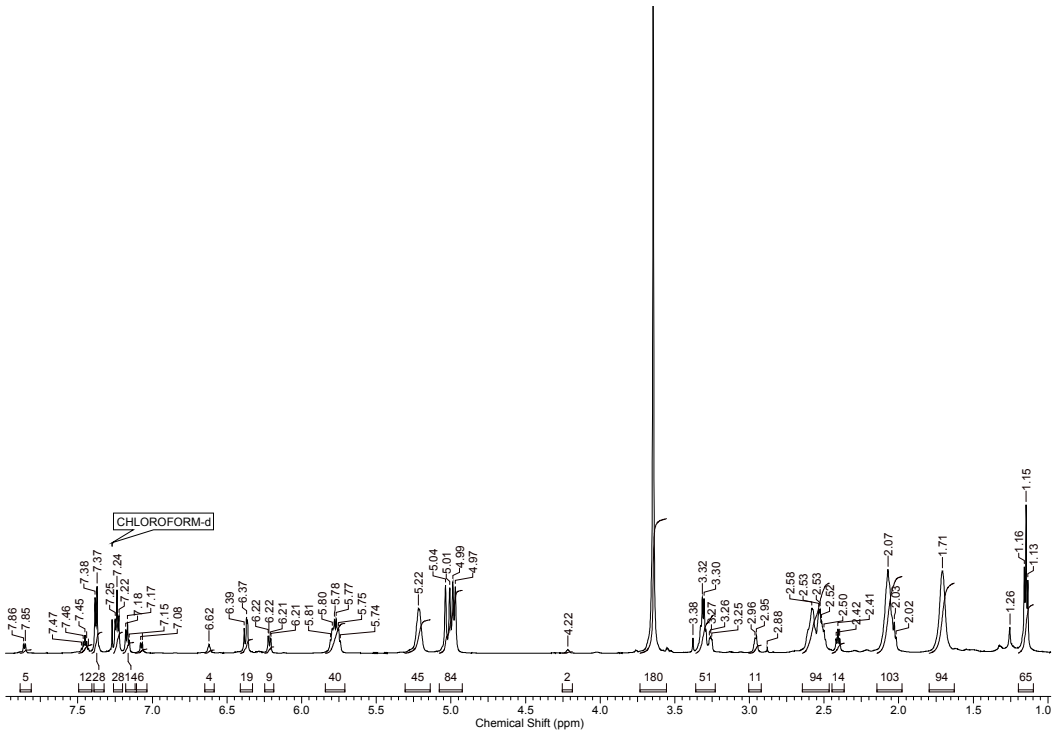

Figure S12. ^{1}H NMR spectrum of PEO_{45}-b-$PHEL_{40}$-RHD_5 (600 MHz, $CDCl_3$).

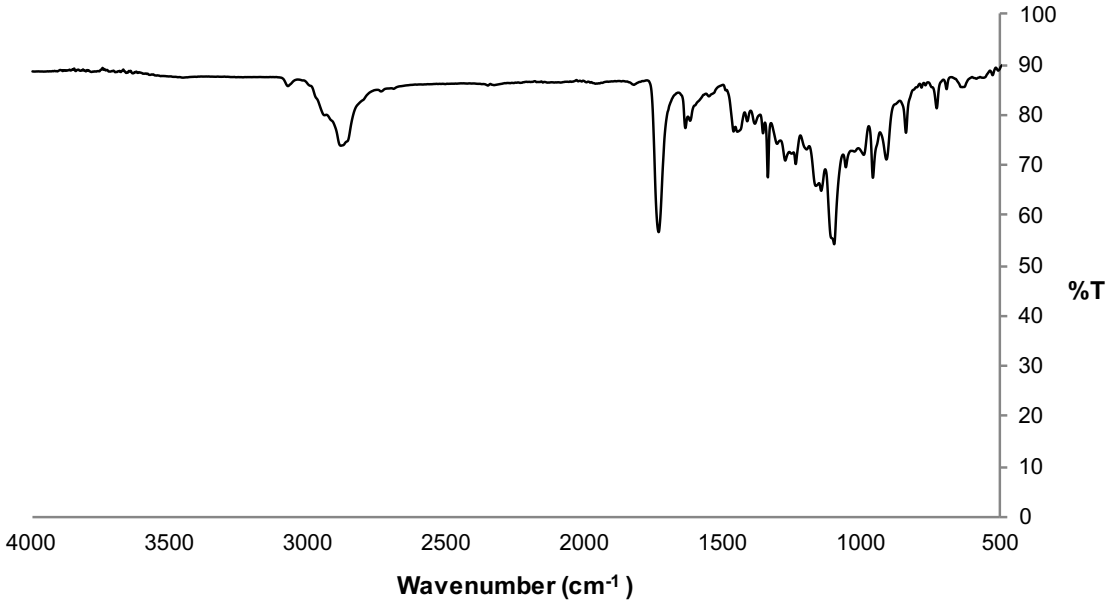

Figure S13. ATR-FTIR spectrum of PEO_{45}-*b*-$PHEL_{23}$.

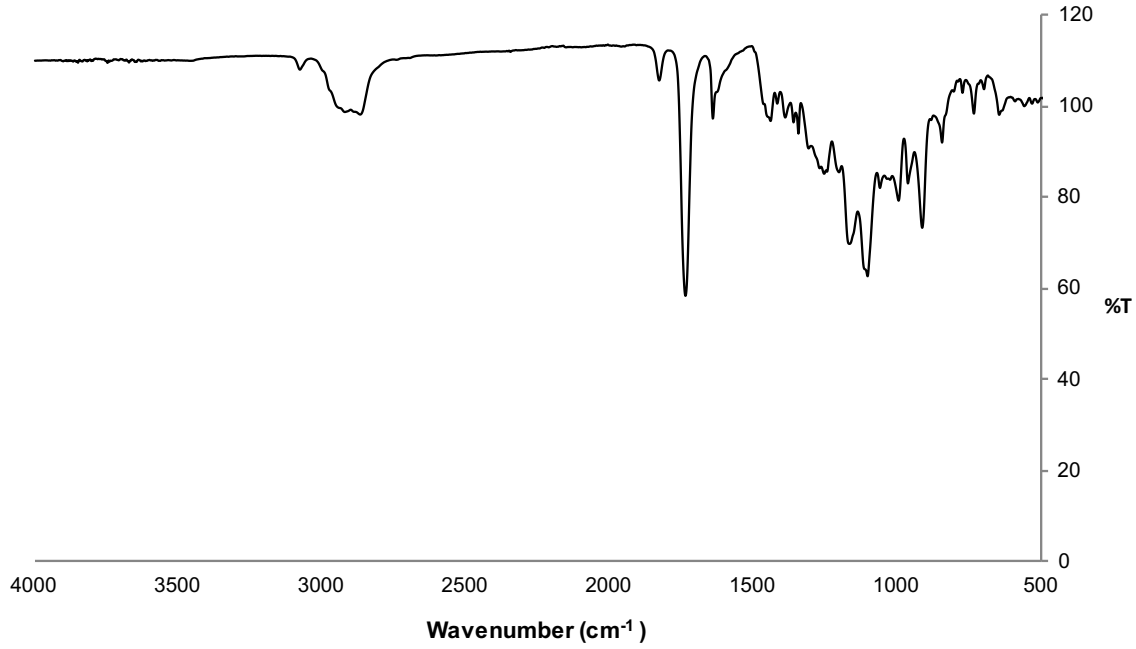

Figure S14. ATR-FTIR spectrum of PEO_{45}-*b*-$PHEL_{45}$.

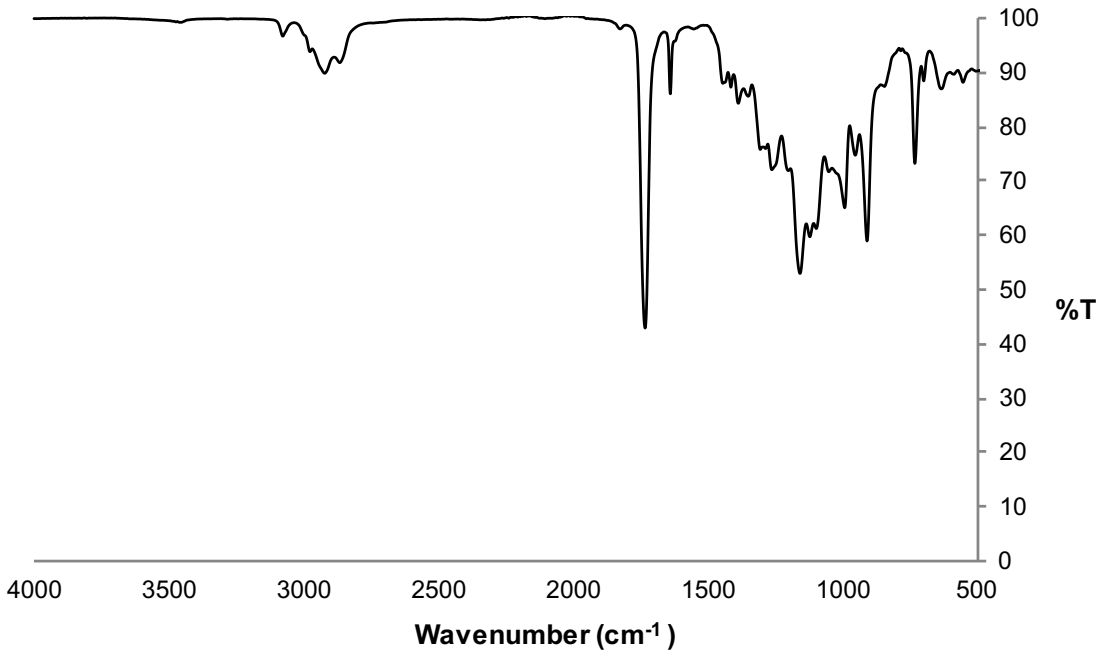

Figure S15. ATR-FTIR spectrum of PEO_{45}-*b*-$PHEL_{79}$.

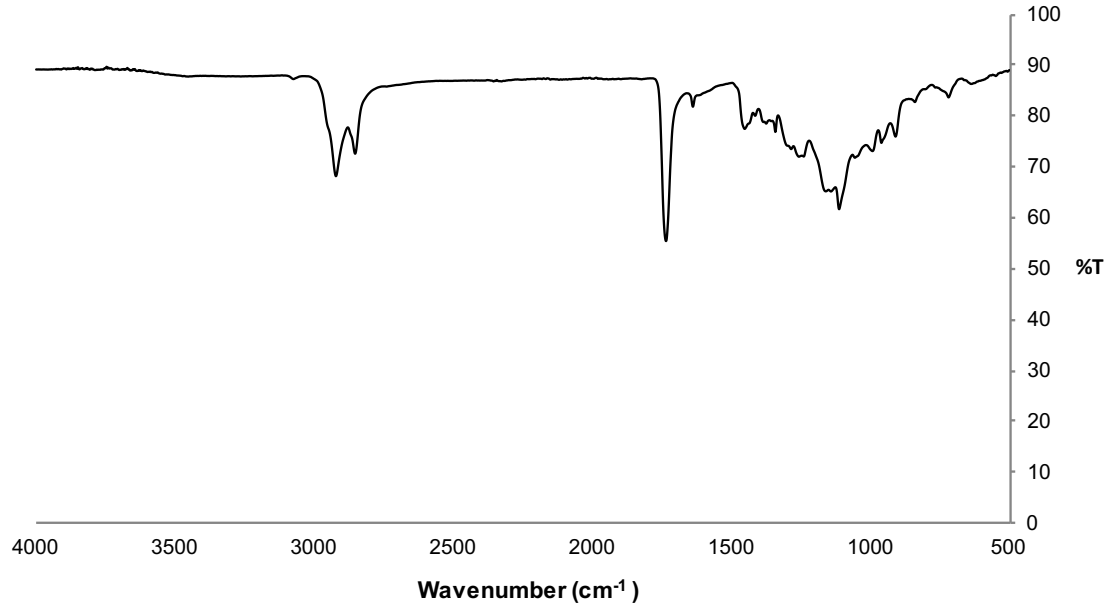

Figure S16. ATR-FTIR spectrum of PEO_{45}-*b*-$PHEL_{21}$-$octyl_{24}$.

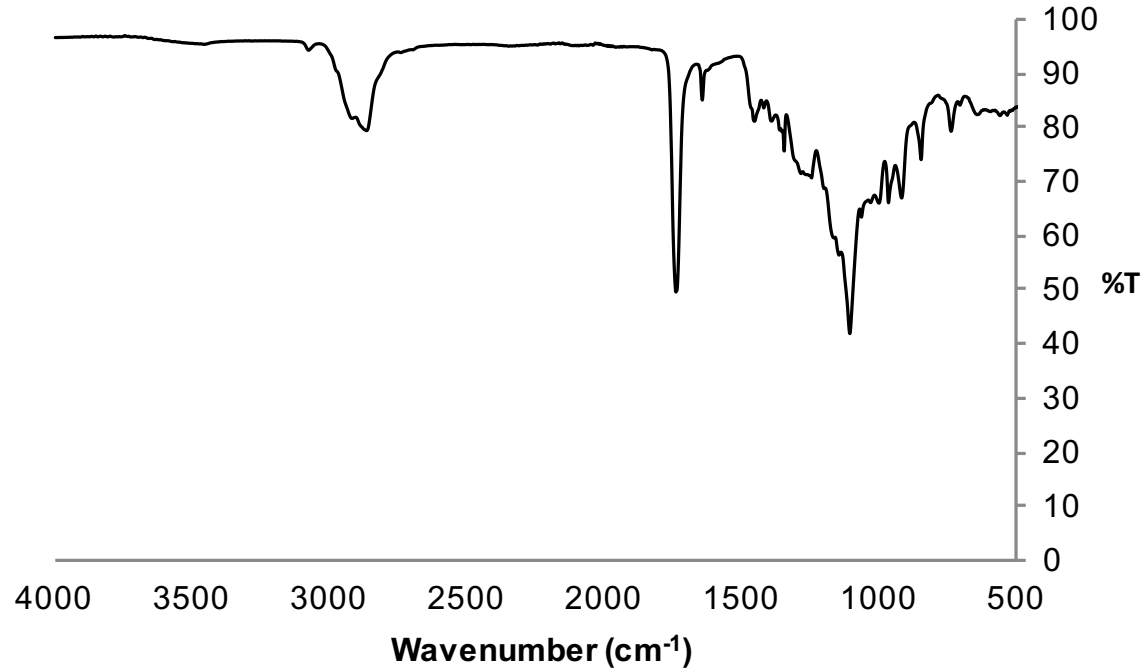

Figure S17. ATR-FTIR spectrum of PEO_{45}-*b*-$PHEL_{31}$-TEG_{14}.

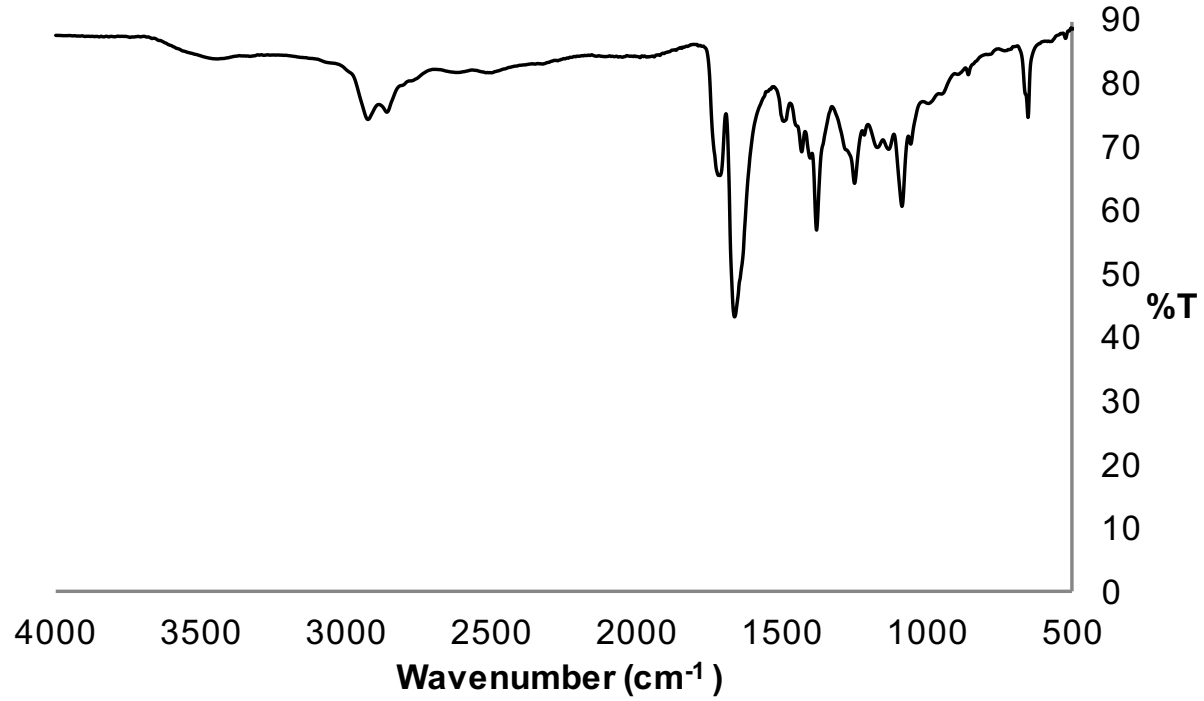

Figure S18. ATR-FTIR spectrum of PEO_{45}-*b*-CA_{45}.

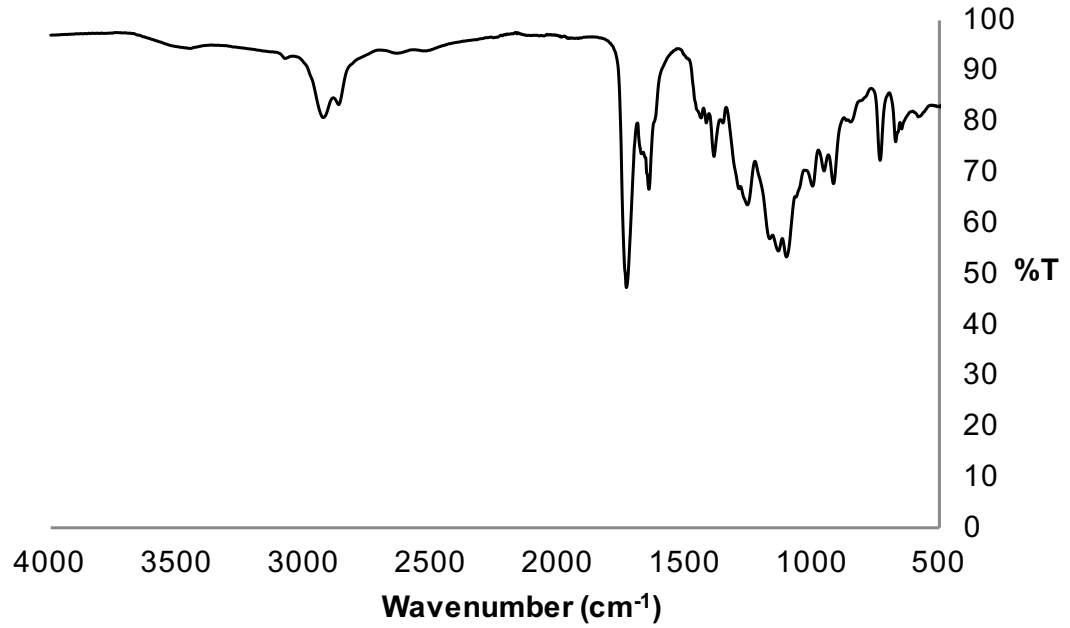

Figure S19. ATR-FTIR spectrum of PEO_{45}-*b*-$PHEL_{20}$-CA_{25}.

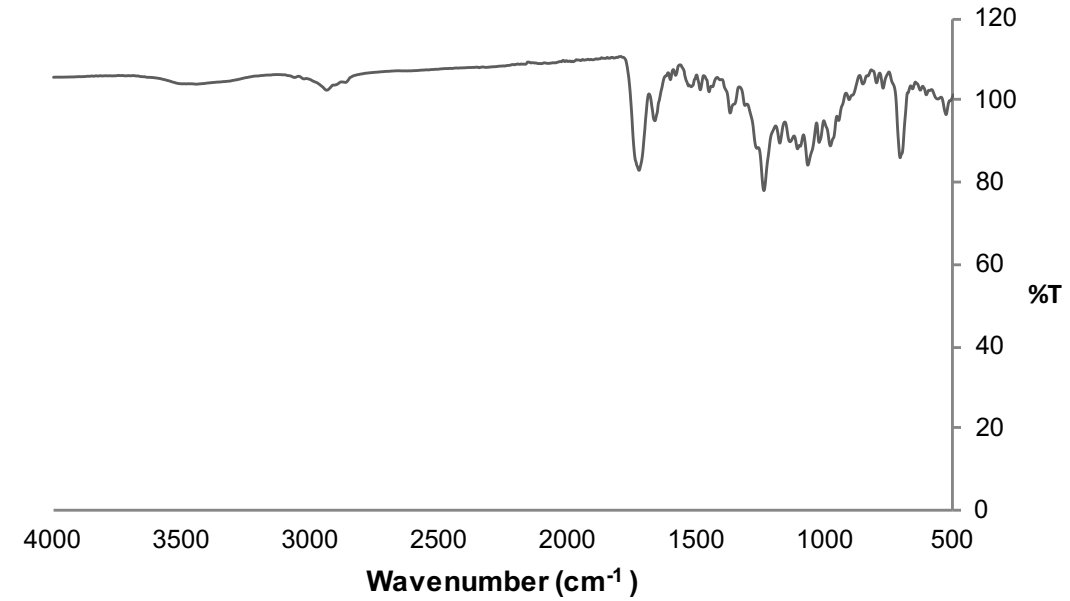

Figure S20. ATR-FTIR spectrum of PEO_{45}-*b*-CA_{11}-PTX_{34}.

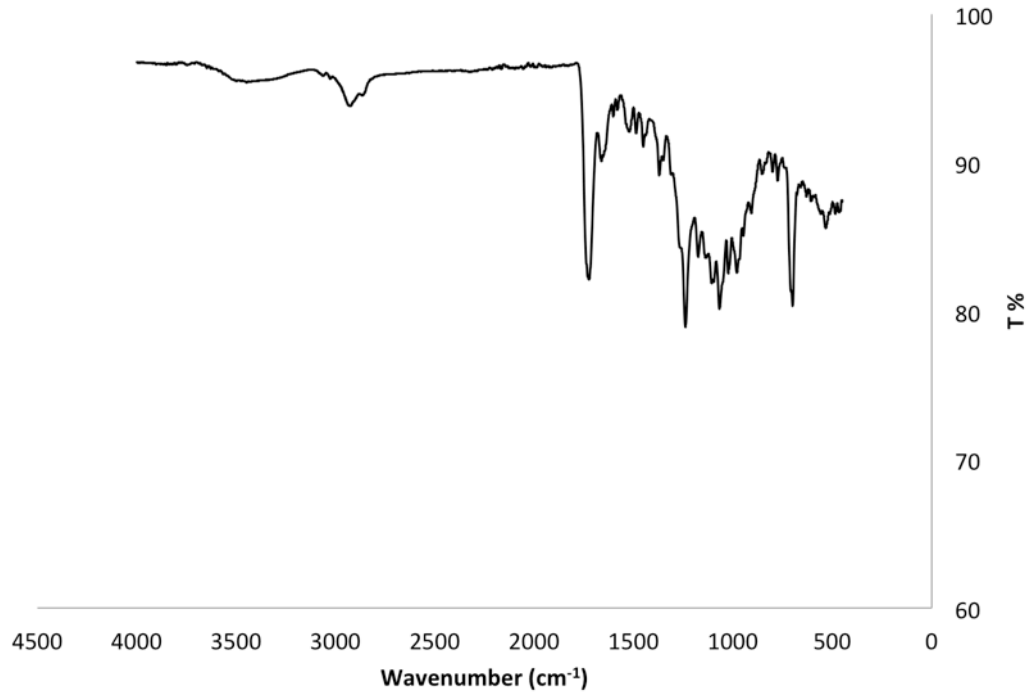

Figure S21. ATR-FTIR spectrum of PEO_{45}-*b*-$PHEL_{20}$-CA_7-PTX_{18}.

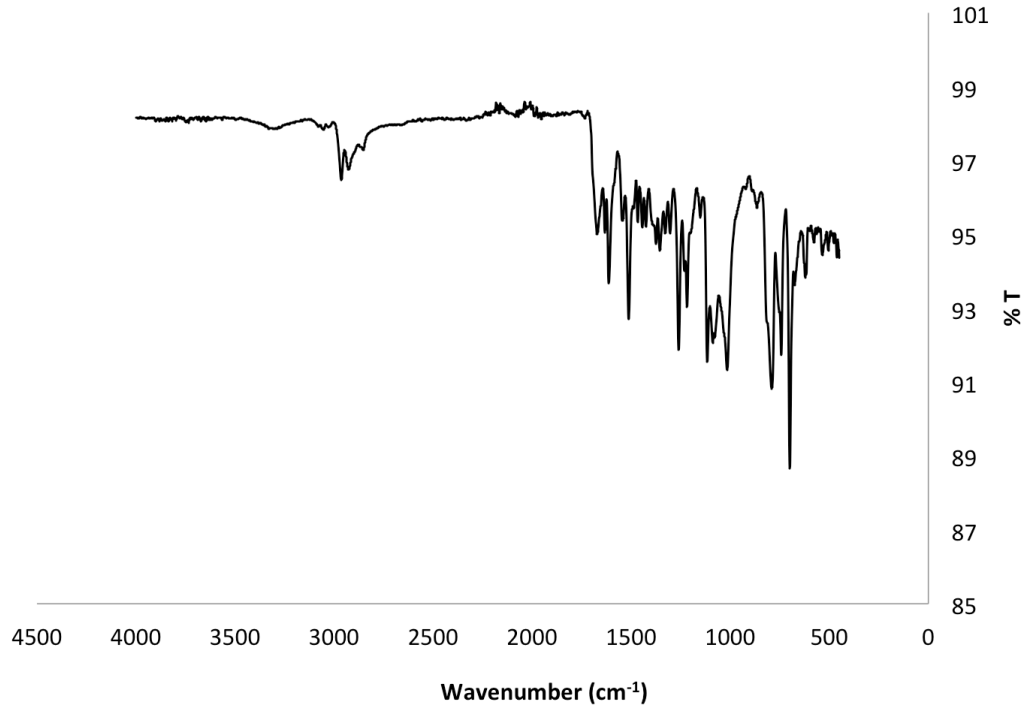

Figure S22. ATR-FTIR spectrum of **4**.

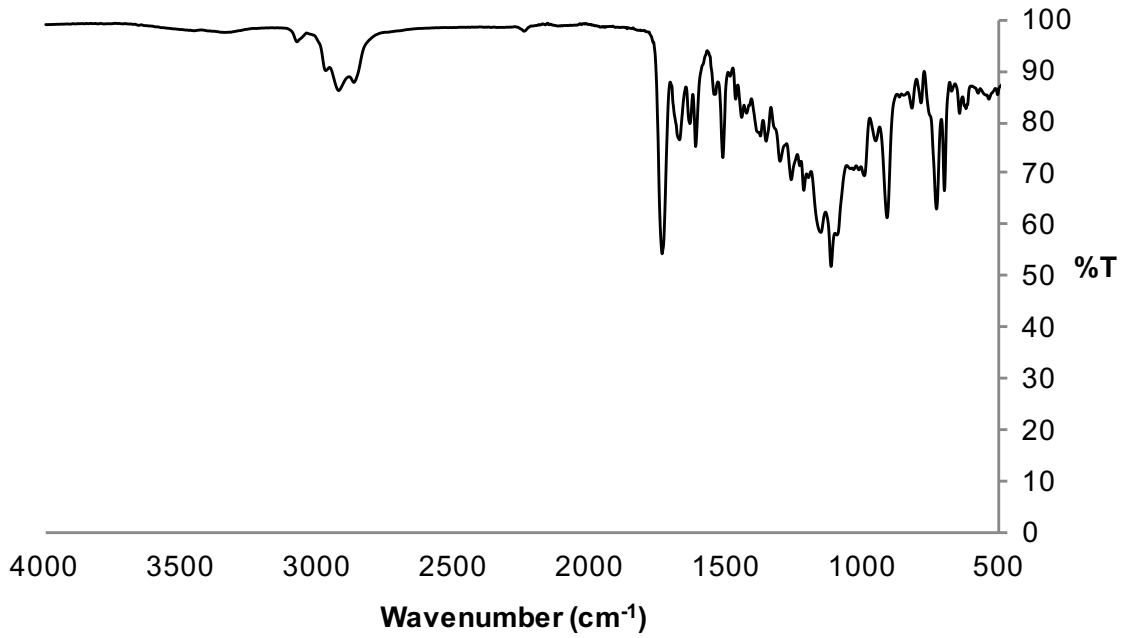

Figure S23. ATR-FTIR spectra of PEO_{45}-*b*-$PHEL_{40}$-RHD_5.

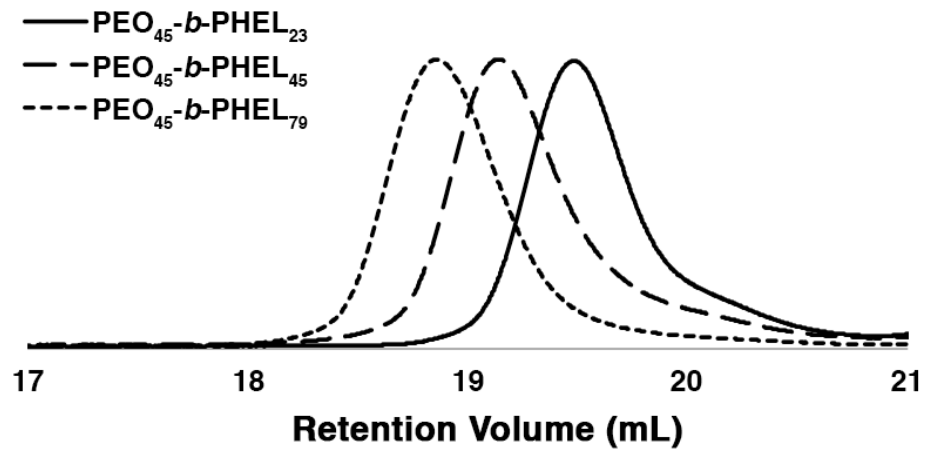

Figure S24. SEC traces for PEO_{45}-*b*-$PHEL_{23}$, PEO_{45}-*b*-$PHEL_{45}$ and PEO_{45}-*b*-$PHEL_{79}$ (THF, refractive index detection).

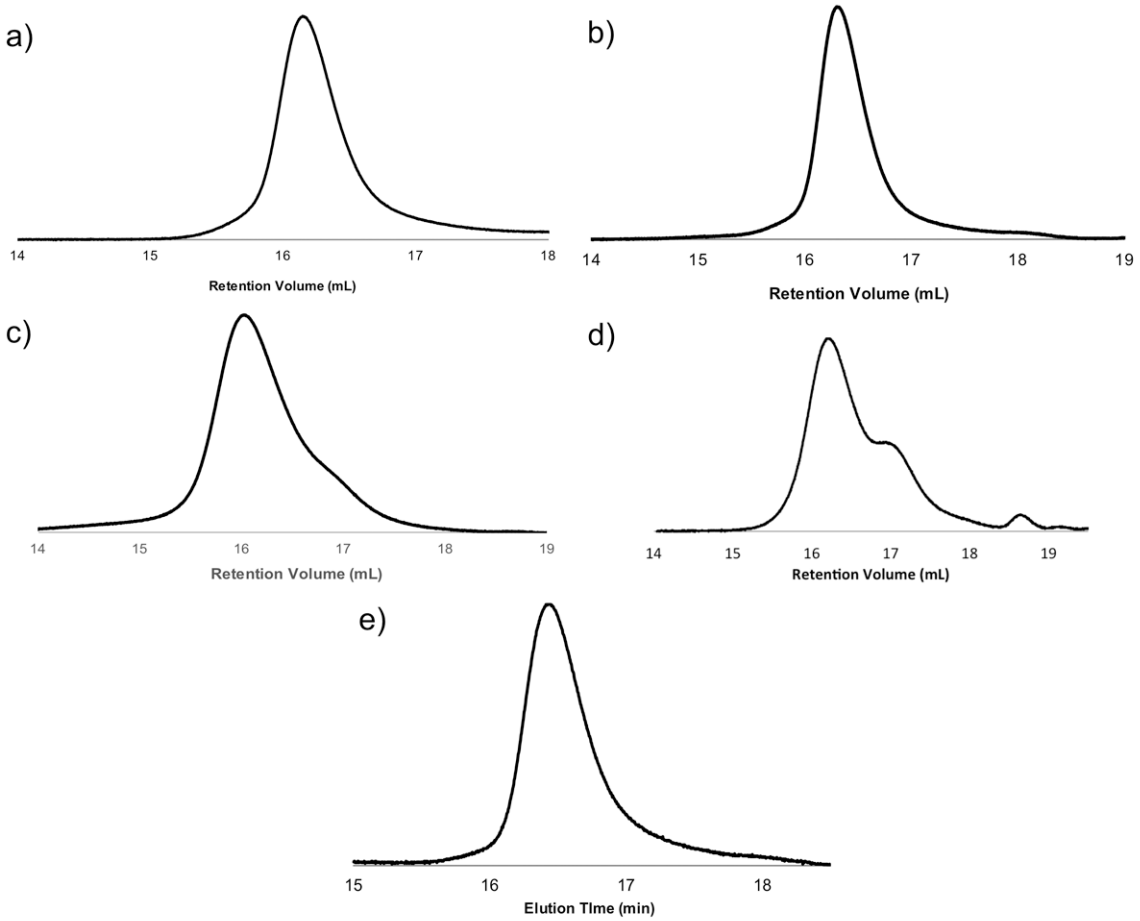

Figure S25. SEC traces (THF, refractive index detection) for: a) PEO_{45}-*b*-$PHEL_{21}$-$octyl_{24}$, b) PEO_{45}-*b*-$PHEL_{31}$-TEG_{14}, c) PEO_{45}-*b*-CA_{11}-PTX_{34}, d) PEO_{45}-*b*-$PHEL_{20}$-CA_7-PTX_{18}, e) PEO_{45}-*b*-$PHEL_{40}$-RHD_5.

Table S1. Summary of the onset degradation temperatures (T_o) for PEO-*b*-PHEL and its derivatives as measured by TGA.

Polymer	T_o (°C)
PEO_{45}-*b*-$PHEL_{23}$	262
PEO_{45}-*b*-$PHEL_{45}$	257
PEO_{45}-*b*-$PHEL_{79}$	262
PEG_{45}-*b*-$PHEL_{21}$-$octyl_{24}$	256
PEG_{45}-*b*-$PHEL_{31}$-TEG_{14}	254
PEG_{45}-*b*-CA_{45}	246
PEG_{45}-*b*-CA_{11}-PTX_{34}	221
PEG_{45}-*b*-$PHEL_{20}$-CA_7-PTX_{18}	219
PEG_{45}-*b*-$PHEL_{40}$-RHD_5	247

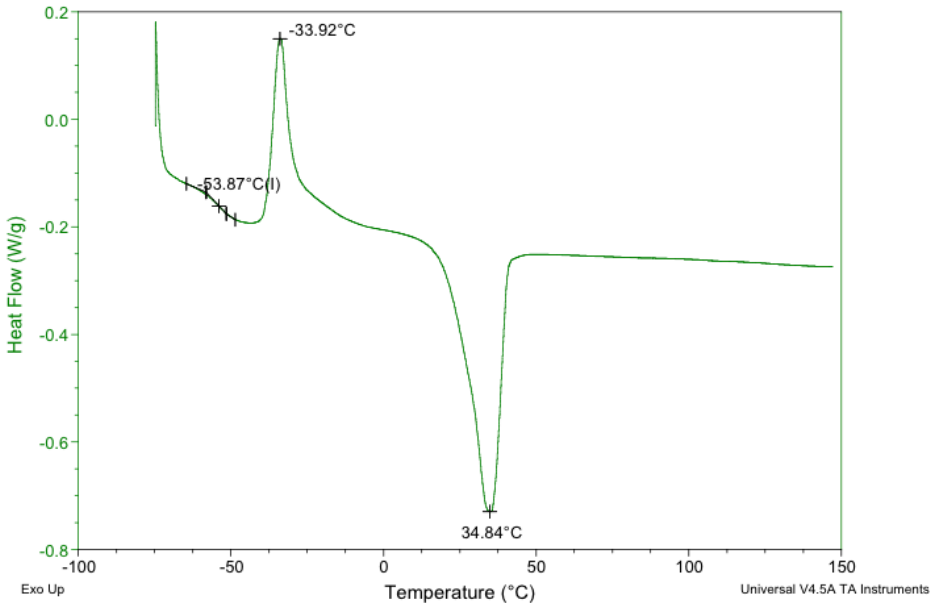

Figure S26. DSC trace for PEO_{45}-*b*-$PHEL_{23}$ (obtained from third heating cycle).

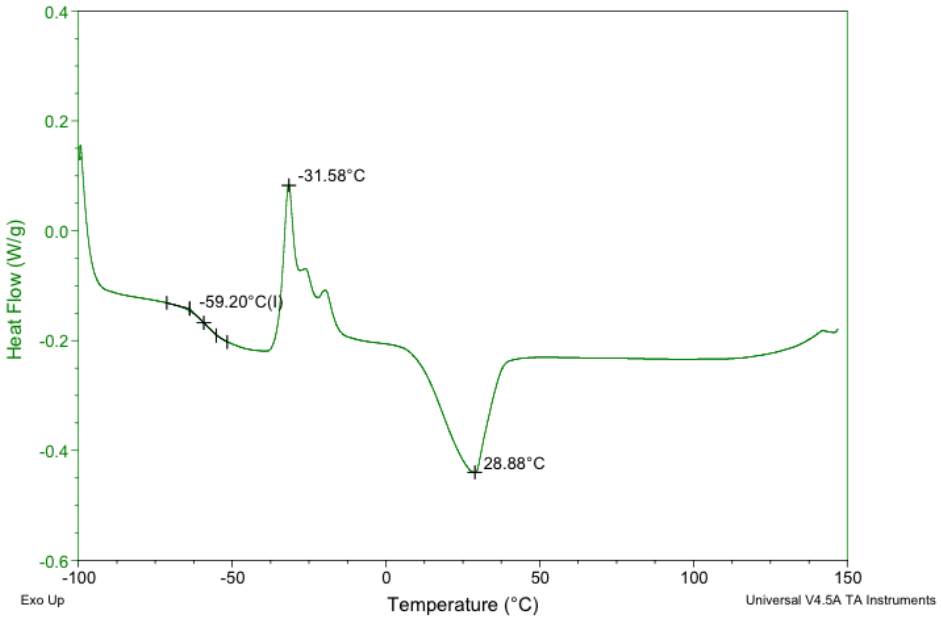

Figure S27. DSC trace for PEO_{45}-*b*-$PHEL_{45}$ (obtained from third heating cycle).

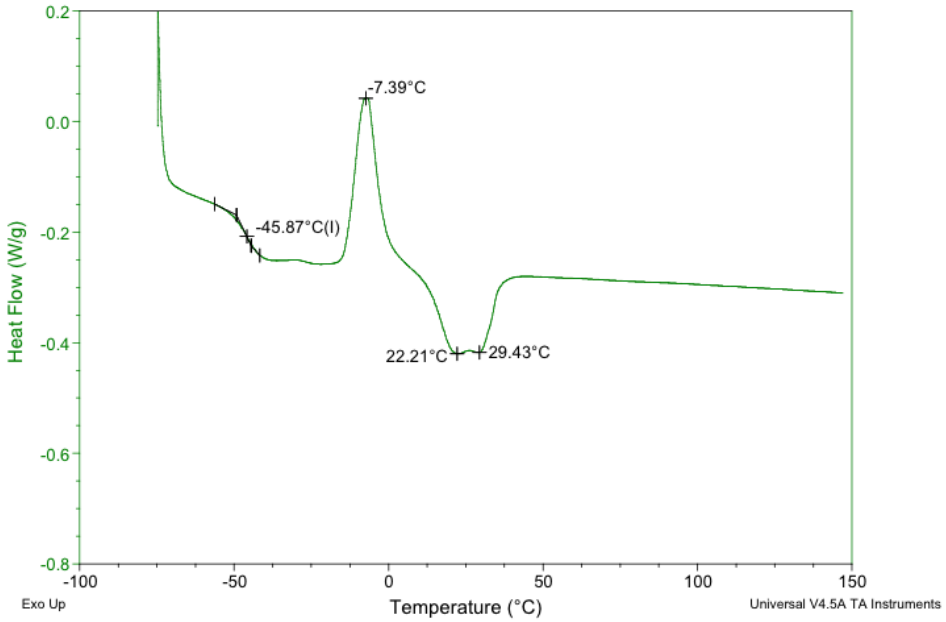

Figure S28. DSC trace for PEO_{45}-*b*-$PHEL_{79}$ (obtained from third heating cycle).

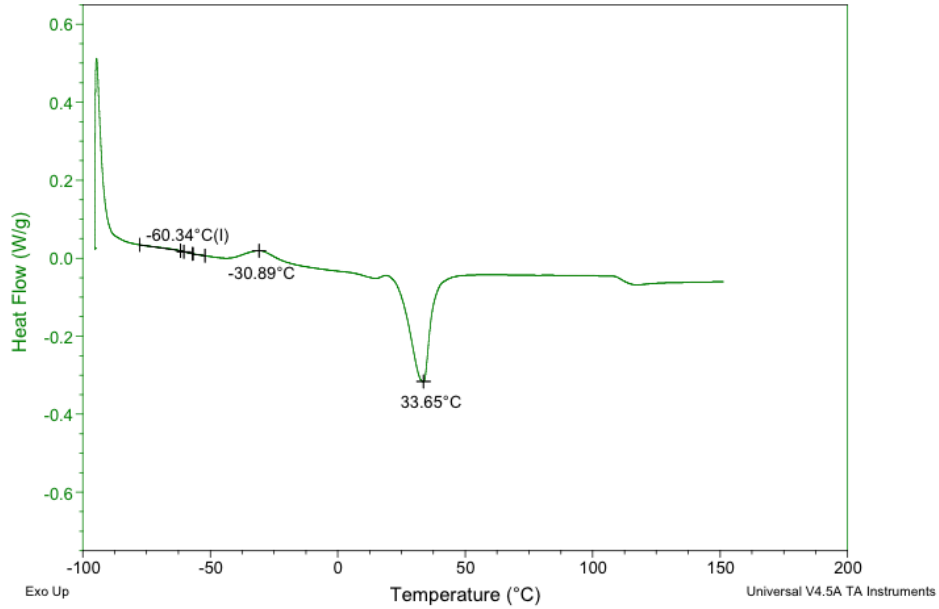

Figure S29. DSC trace for PEO_{45}-*b*-$PHEL_{21}$-$octyl_{24}$ (obtained from fourth heating cycle).

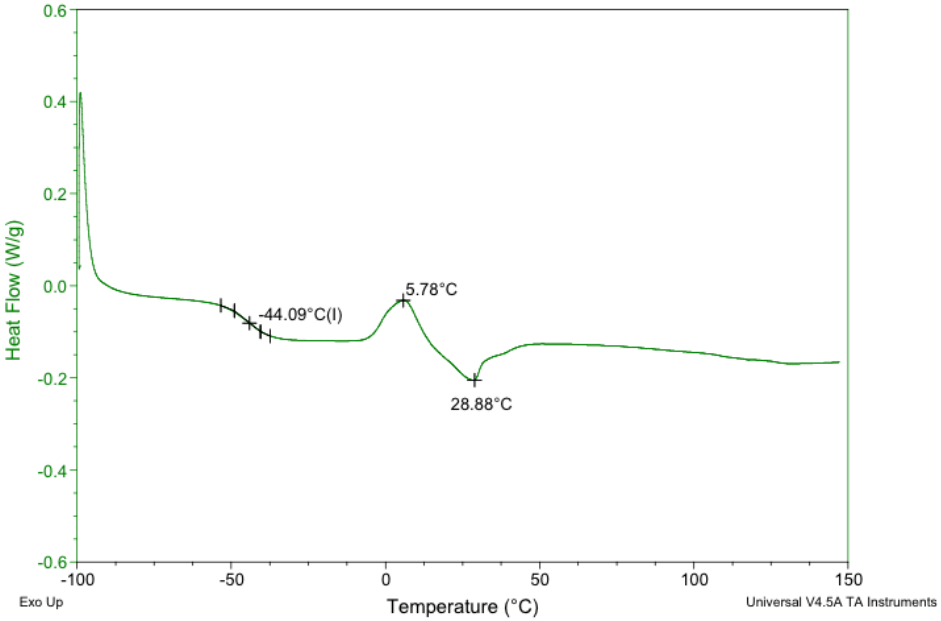

Figure S30. DSC trace for PEO_{45}-*b*-$PHEL_{31}$-TEG_{14} (obtained from fourth heating cycle).

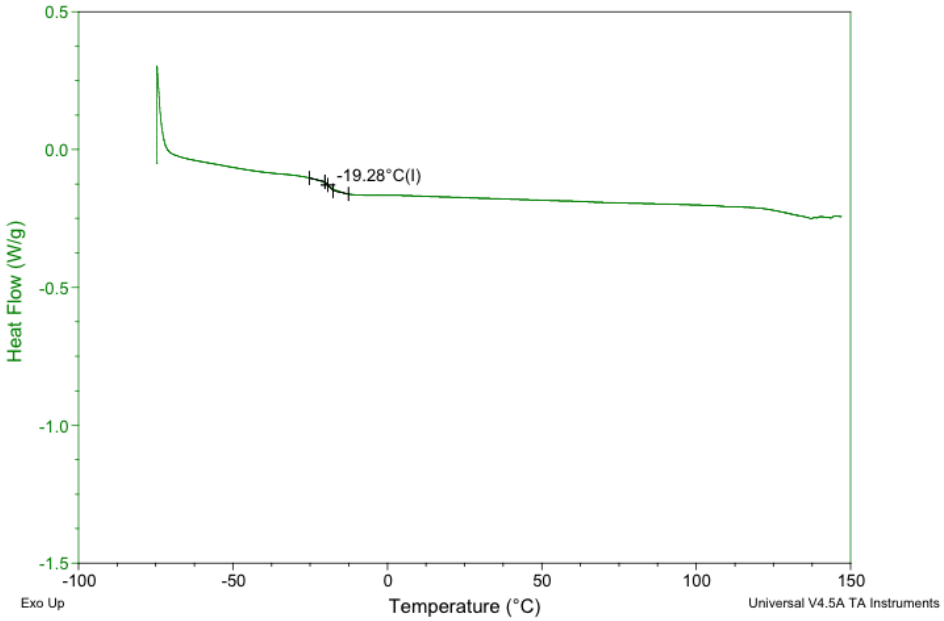

Figure S31. DSC trace for PEO_{45}-*b*-CA_{45} (obtained from third heating cycle).

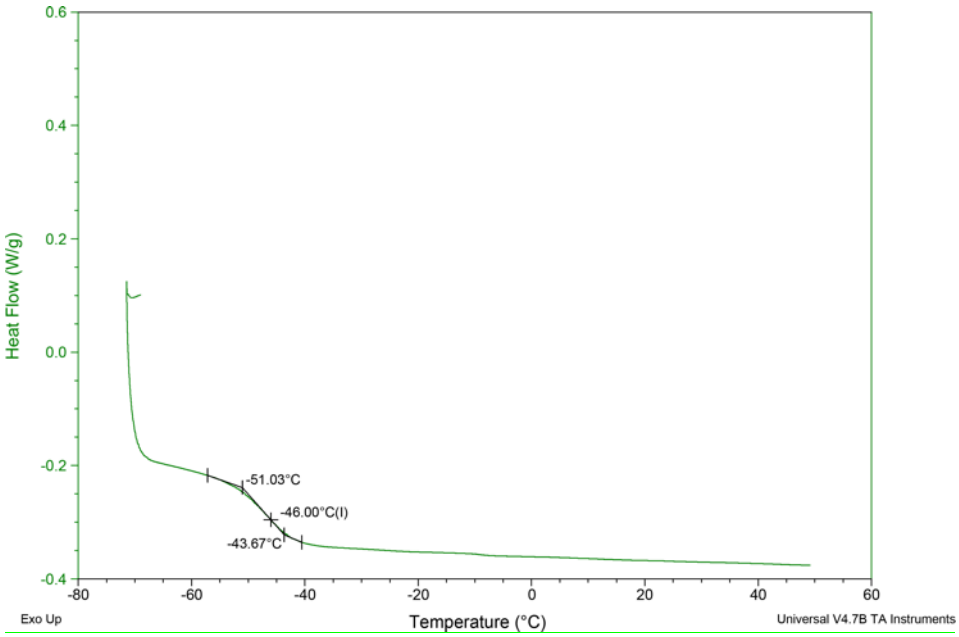

Figure S32. DSC trace for PEO_{45}-*b*-$PHEL_{20}$-CA_{25} (obtained from third heating cycle).

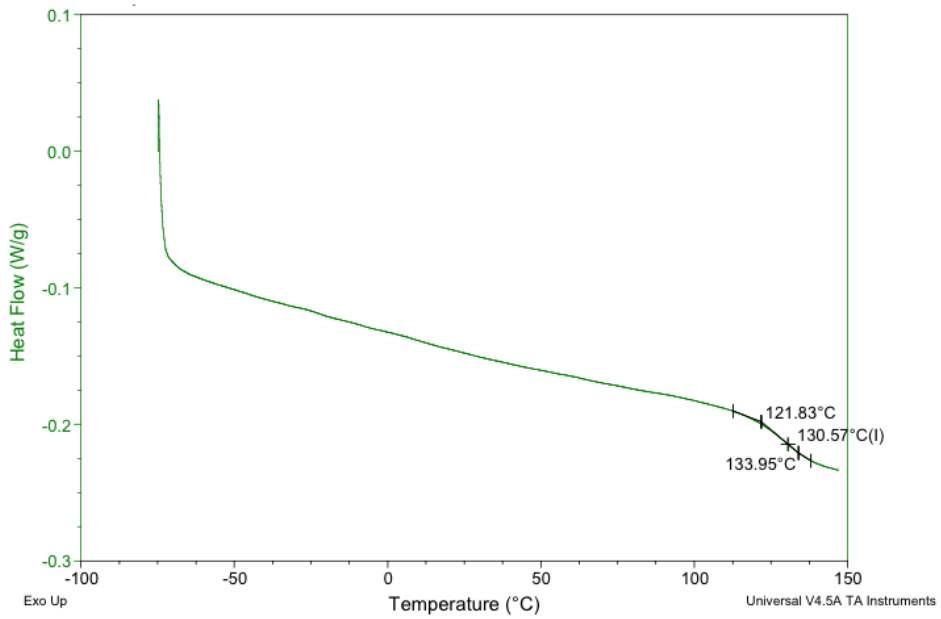

Figure S33. DSC trace for PEO_{45}-*b*-CA_{11}-PTX_{34} (obtained from third heating cycle).

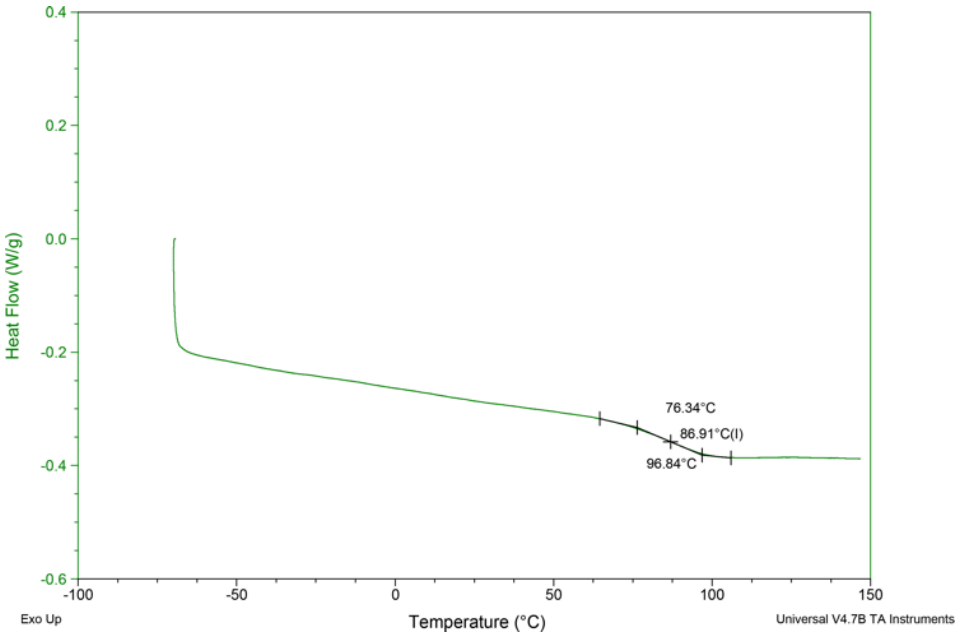

Figure S34. DSC trace for PEO_{45}-*b*-$PHEL_{20}$-CA_7-PTX_{18} (obtained from third heating cycle).

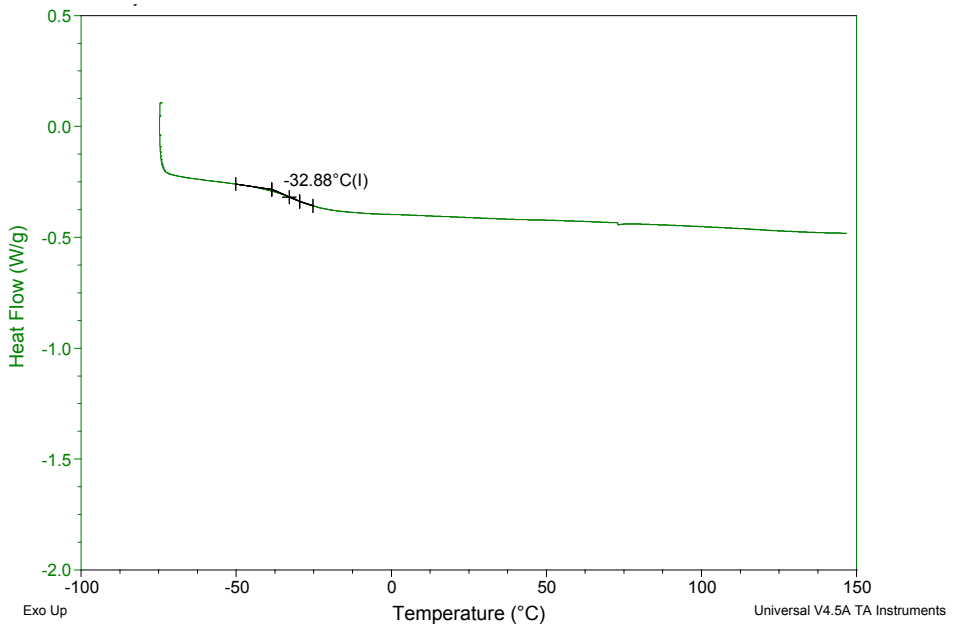

Figure S35. DSC trace for PEO_{45}-*b*-$PHEL_{40}$-RHD_5 (obtained from third heating cycle).

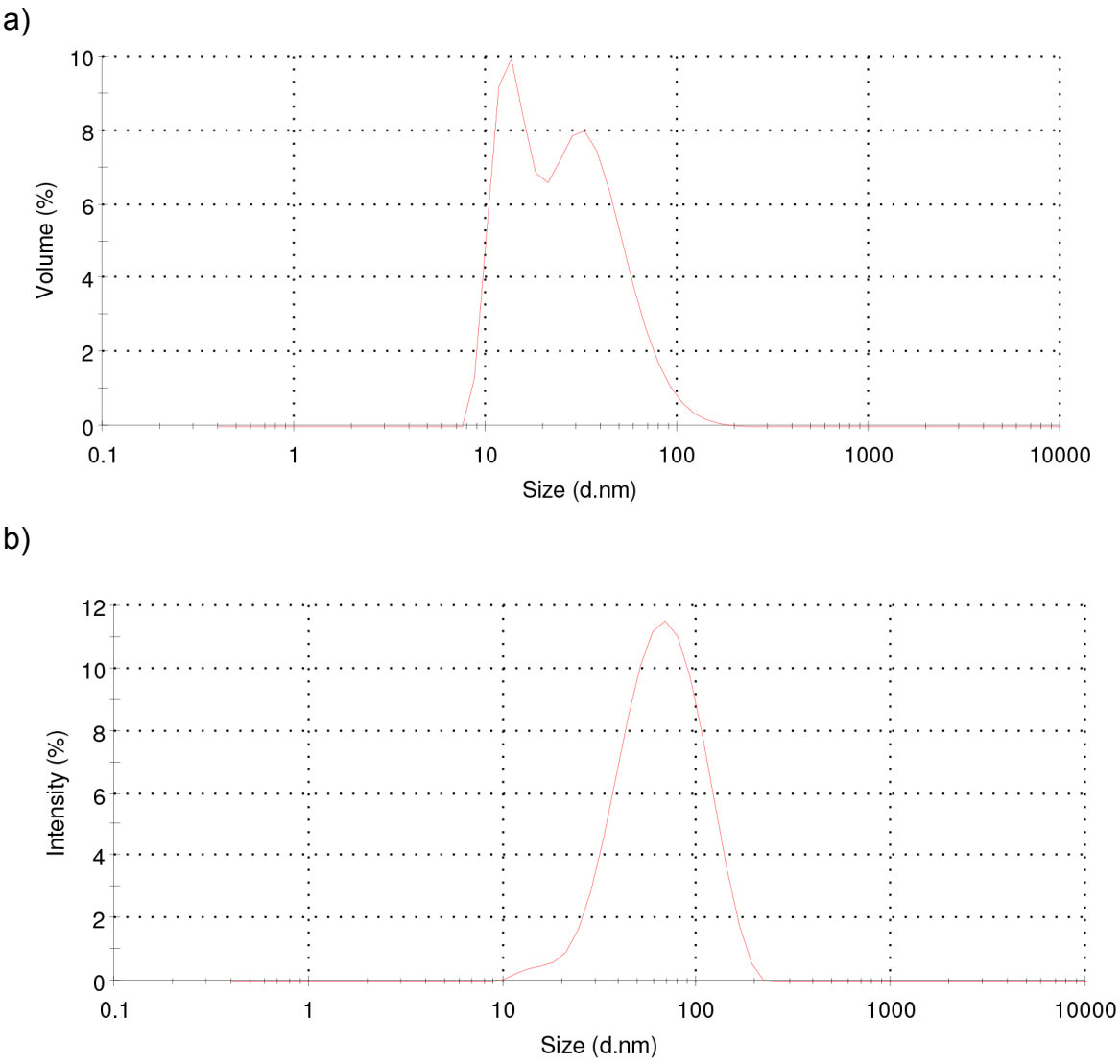

Figure S36. a) Volume and b) intensity distribution of hydrodynamic diameter measured by DLS for PEO_{45}-*b*-$PHEL_{23}$.

a)

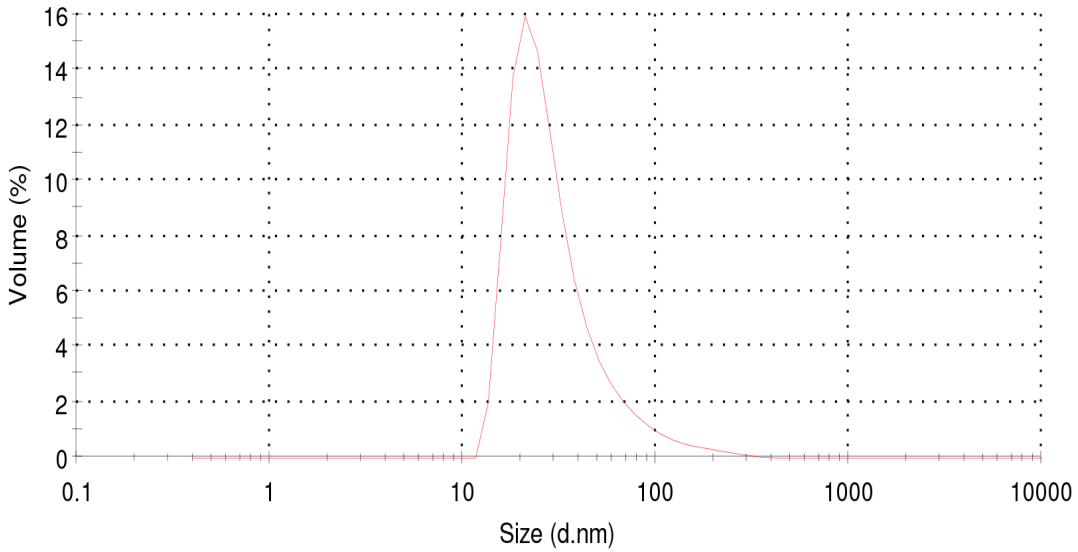

b)

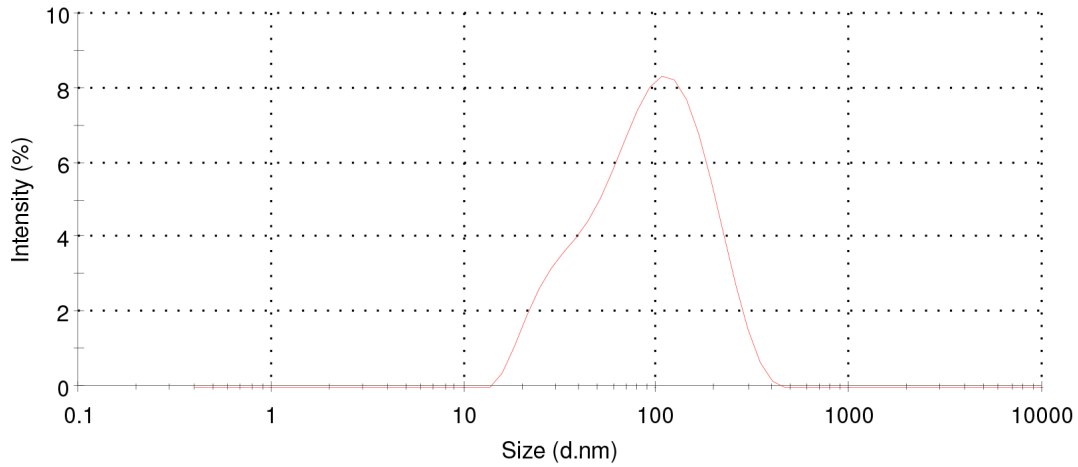

Figure S37. a) Volume and b) intensity distribution of hydrodynamic diameter measured by DLS for PEO_{45}-*b*-$PHEL_{45}$.

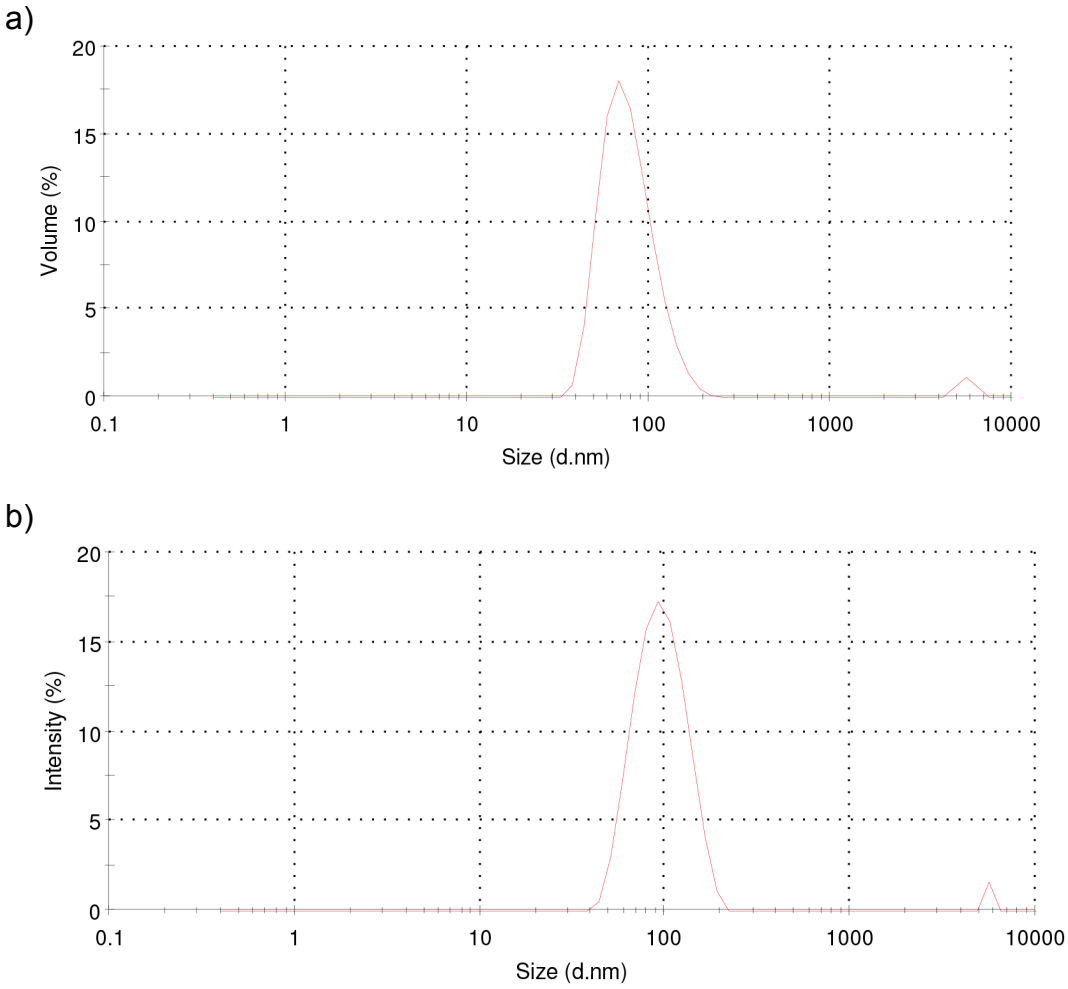

Figure S38. a) Volume and b) intensity distribution of hydrodynamic diameter measured by DLS for PEO_{45}-*b*-$PHEL_{79}$.

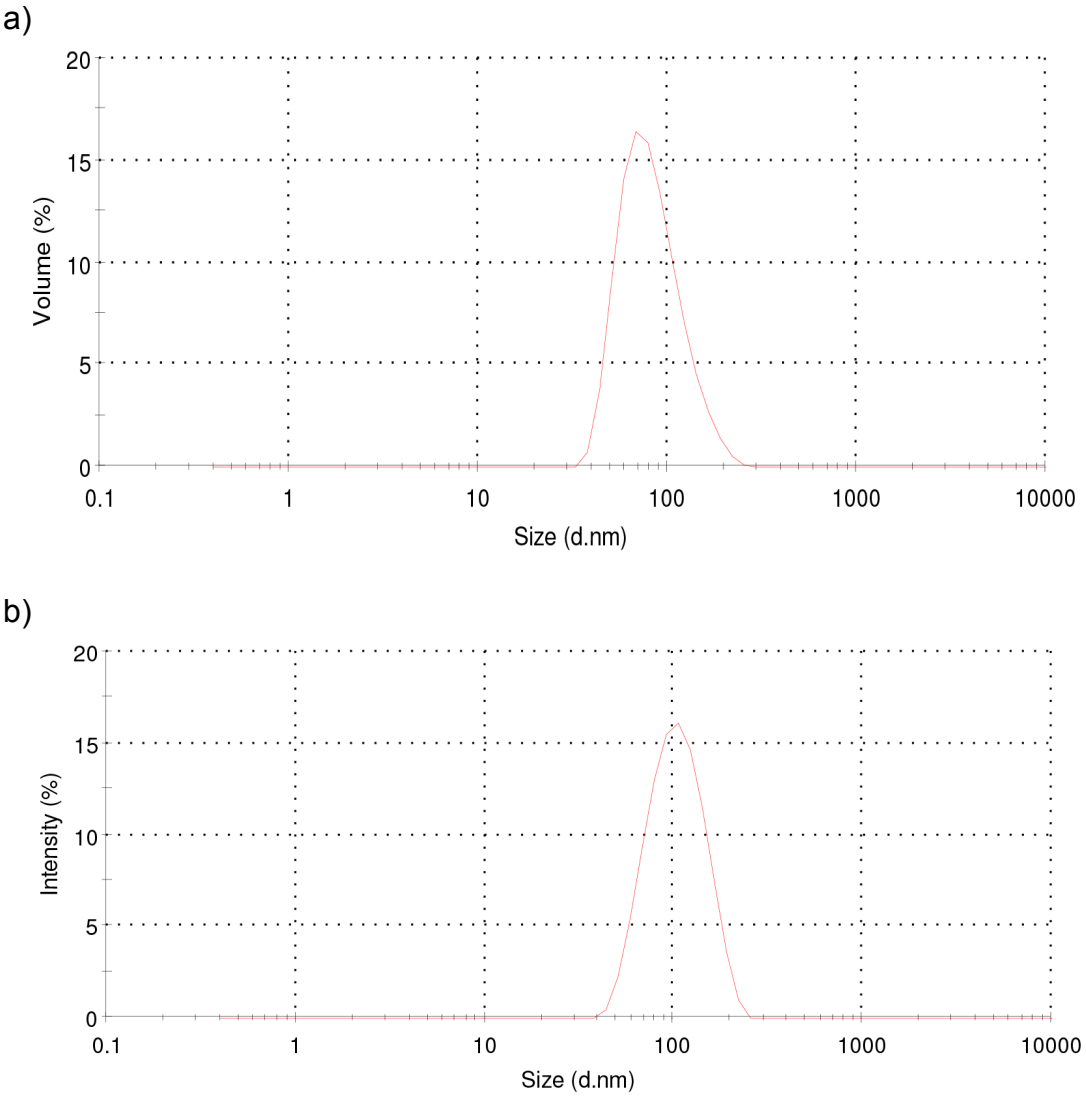

Figure S39. a) Volume and b) intensity distribution of hydrodynamic diameter measured by DLS for PEG_{45}-*b*-$PHEL_{21}$-$octyl_{24}$.

a)

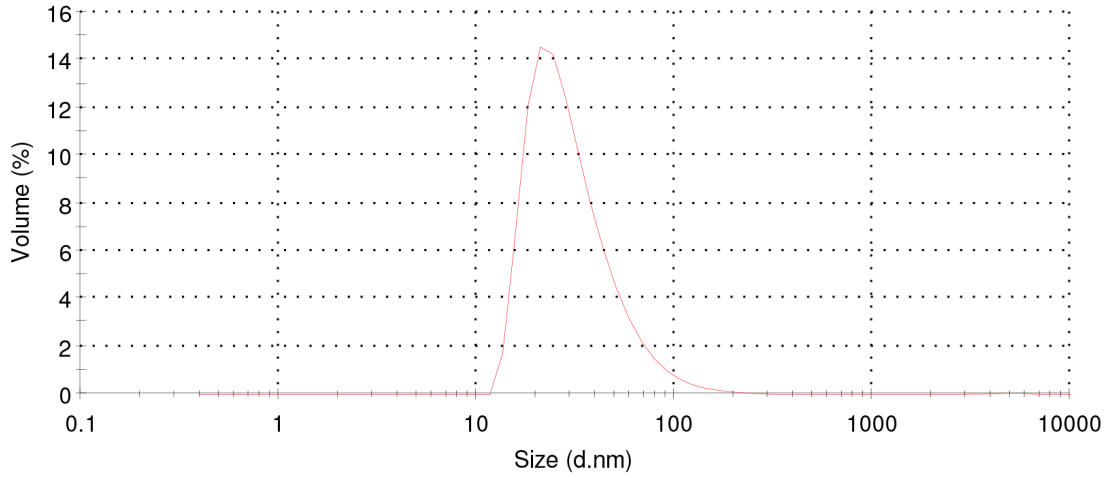

b)

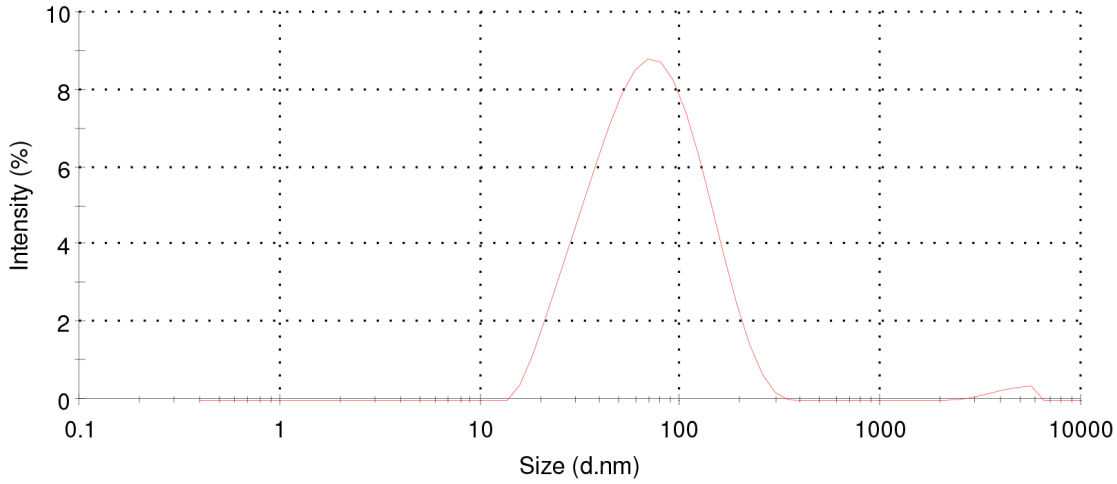

Figure S40. a) Volume and b) intensity distribution of hydrodynamic diameter measured by DLS for PEG_{45}-*b*-$PHEL_{31}$-TEG_{14}.

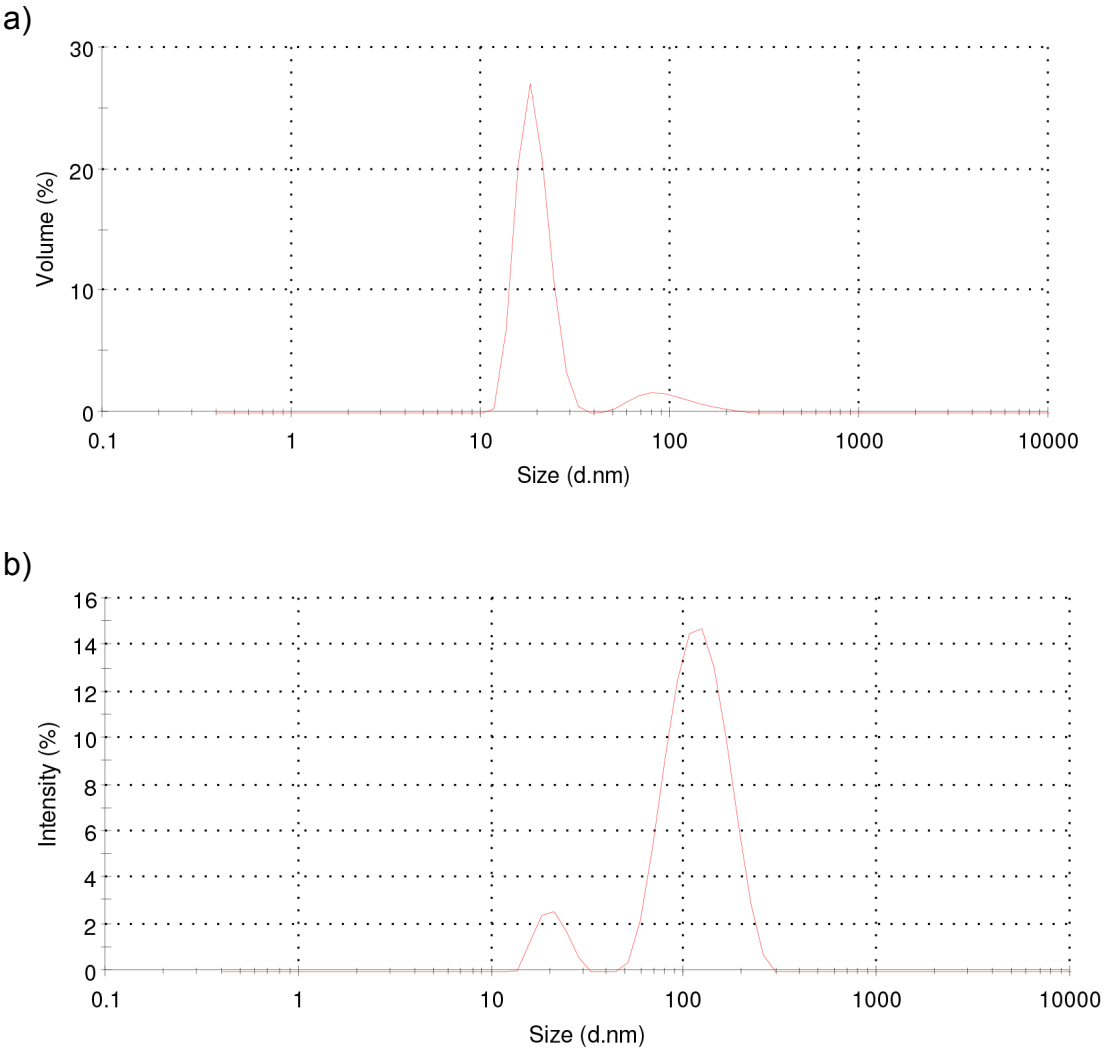

Figure S41. a) Volume and b) intensity distribution of hydrodynamic diameter measured by DLS for PEG_{45}-*b*-$PHEL_{20}$-CA_{25}.

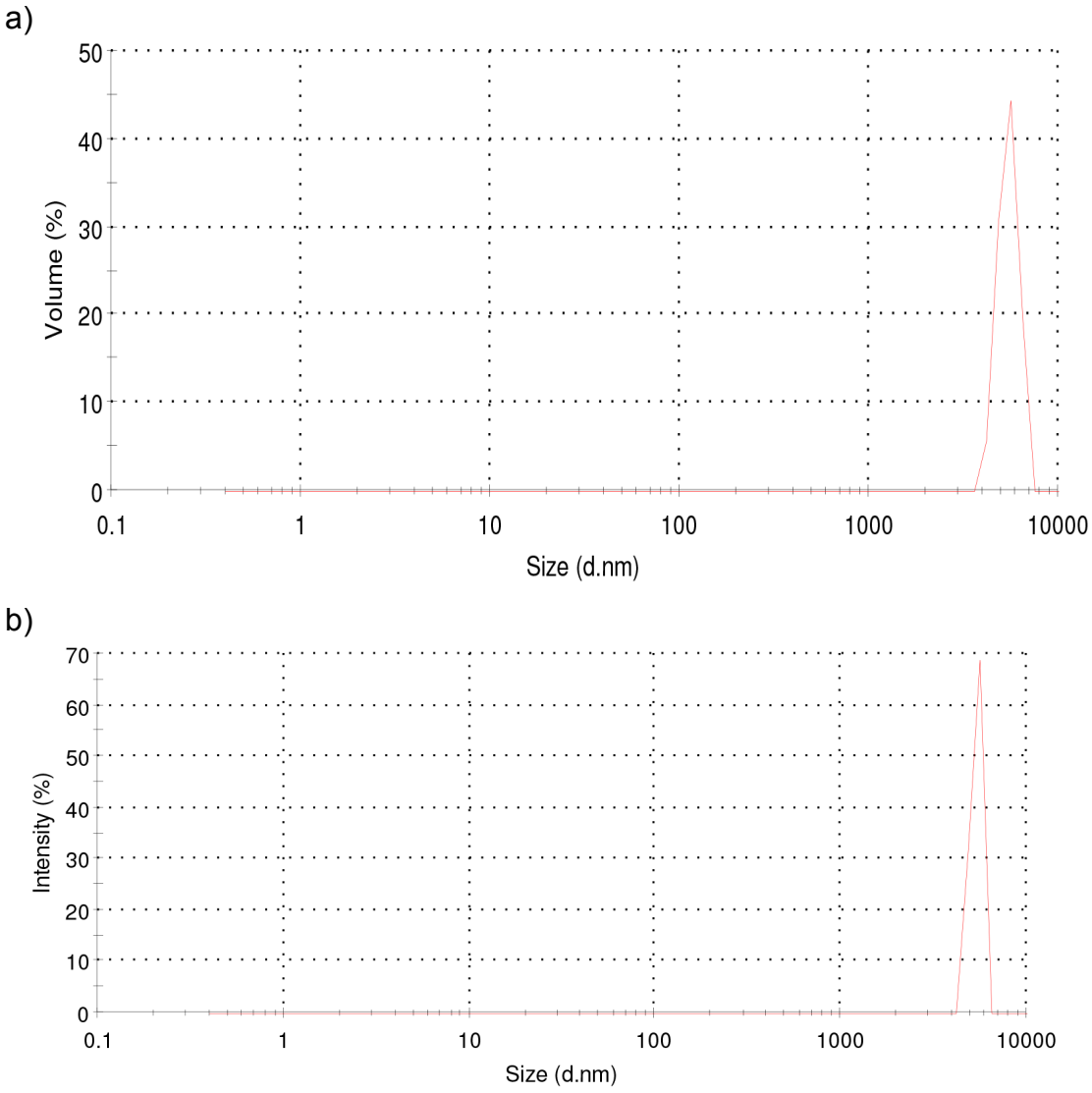

Figure S42. a) Volume and b) intensity distribution of hydrodynamic diameter measured by DLS for PEG_{45}-*b*-$PHEL_{20}$-CA_7-PTX_{18}.

a)

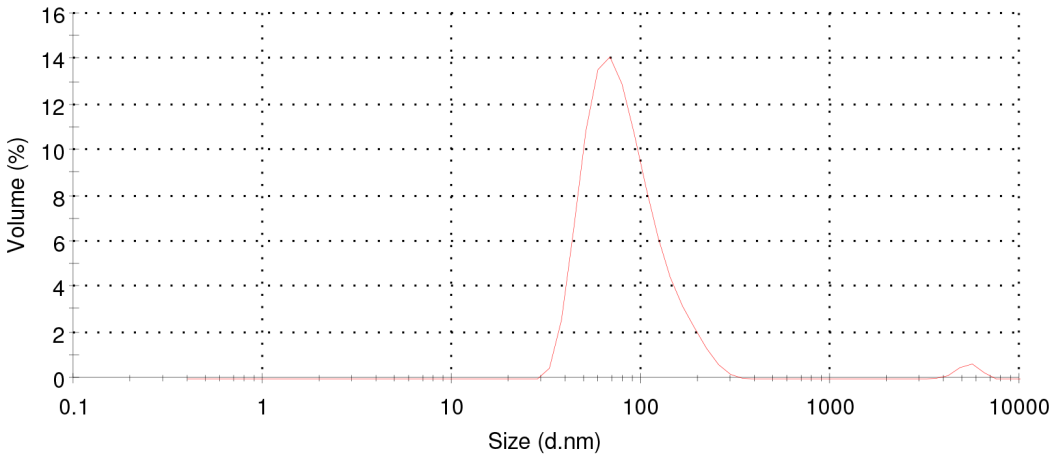

b)

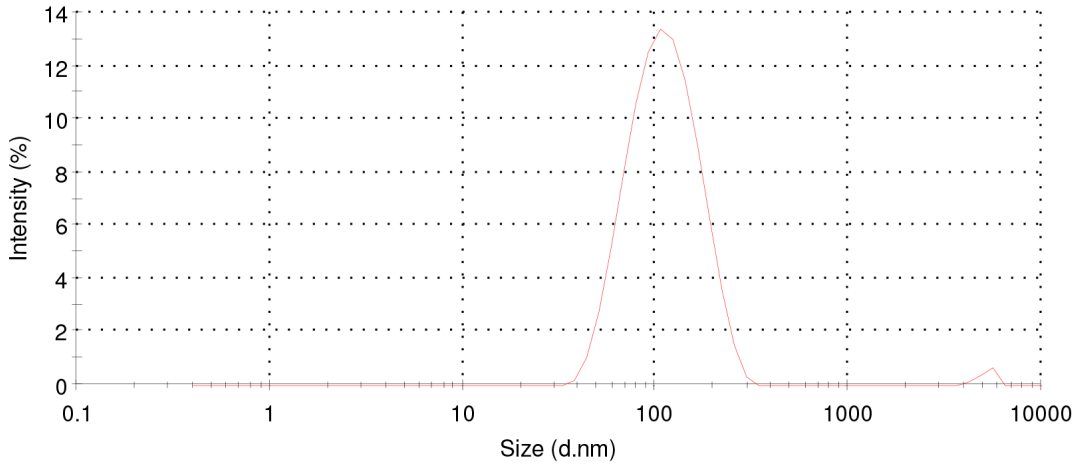

Figure S43. a) Volume and b) intensity distribution of hydrodynamic diameter measured by DLS for PEG_{45}-*b*-$PHEL_{40}$-RHD_5.

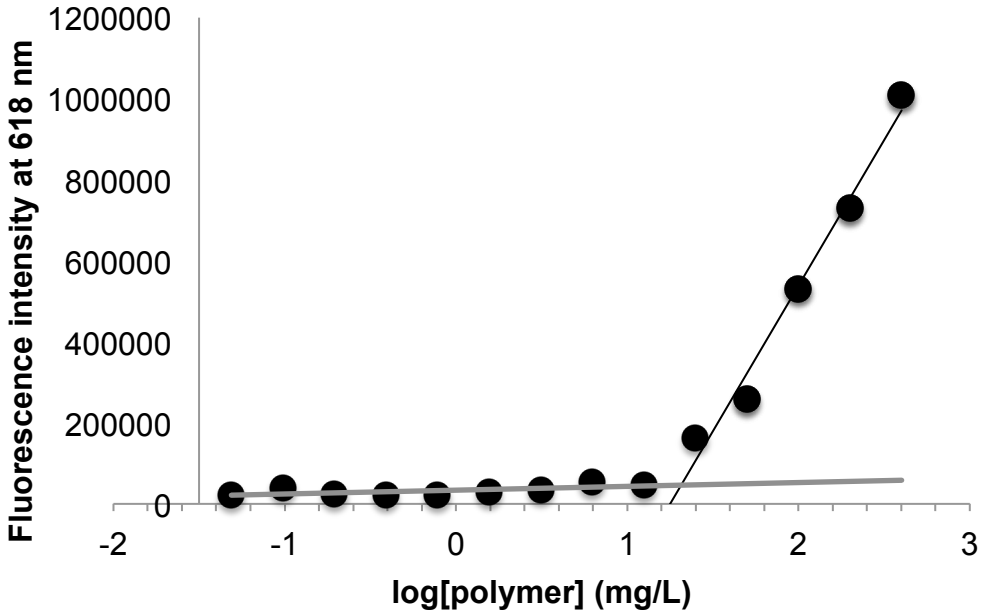

Figure S44. Fluorescence intensity of nile red versus log(concentration of PEO_{45}-*b*-$PHEL_{23}$). The intersection of the two linear regions provides the CAC.

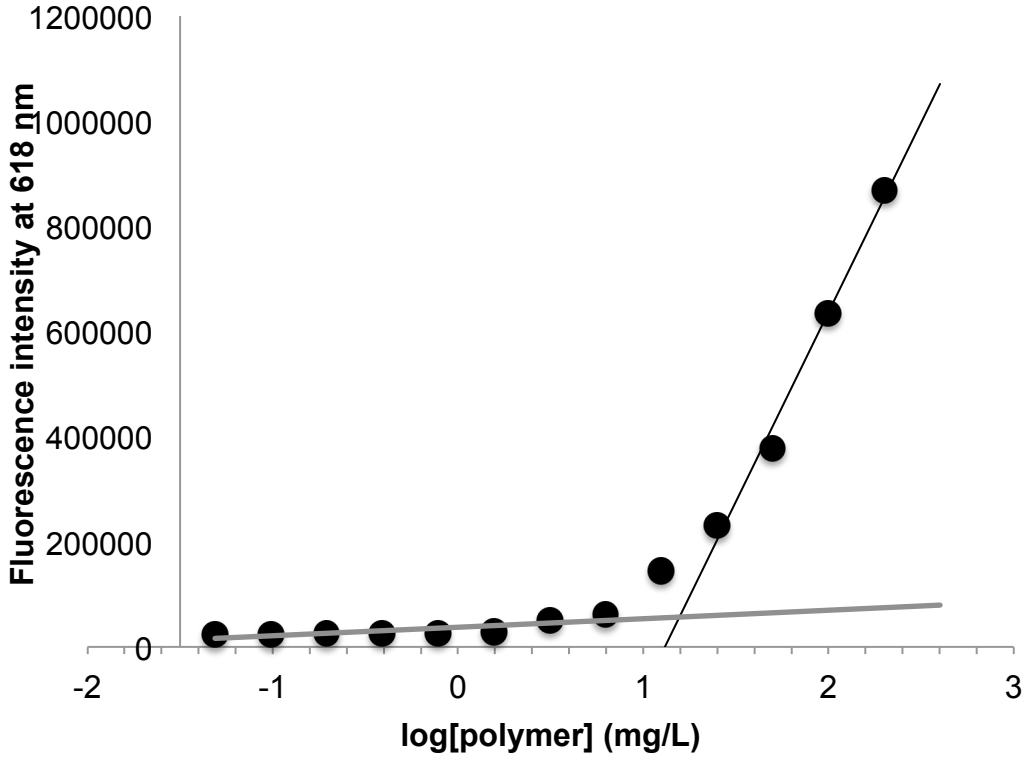

Figure S45. Fluorescence intensity of nile red versus log(concentration of PEO_{45}-*b*-$PHEL_{45}$). The intersection of the two linear regions provides the CAC.

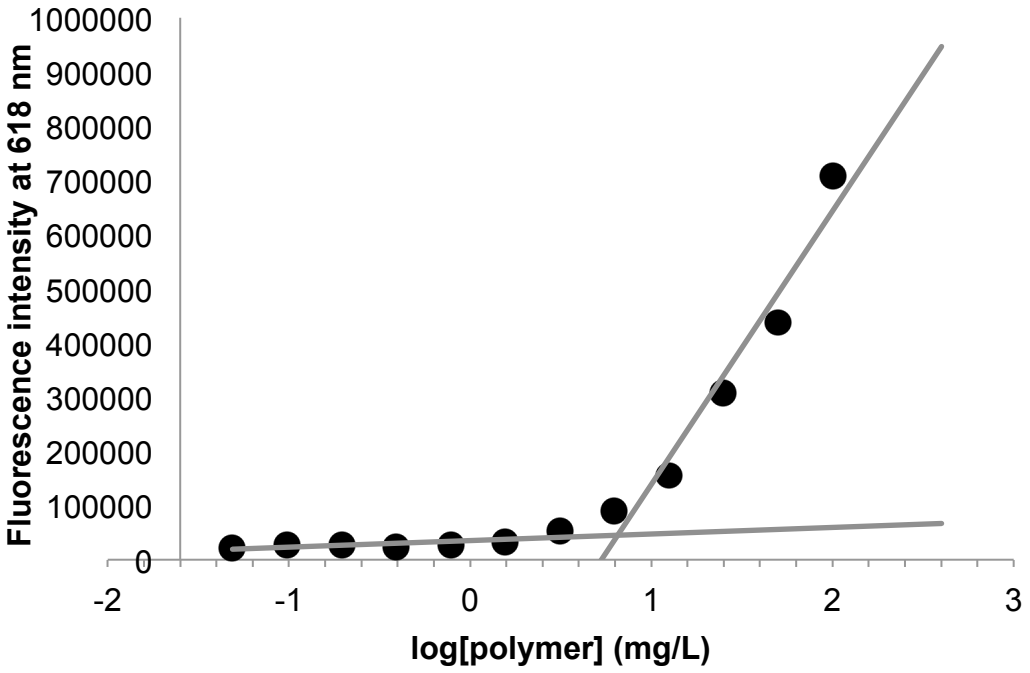

Figure S46. Fluorescence intensity of nile red versus log(concentration of PEO_{45}-*b*-$PHEL_{79}$). The intersection of the two linear regions provides the CAC.

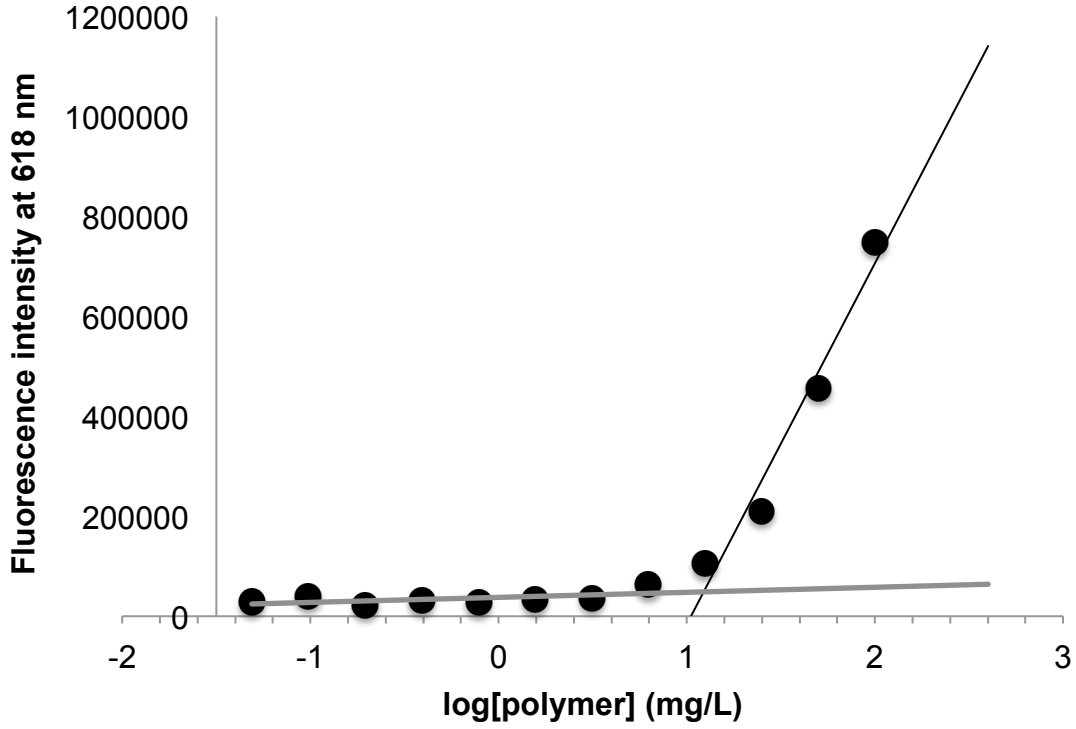

Figure S47. Fluorescence intensity of nile red versus log(concentration of PEO_{45}-*b*-$PHEL_{21}octyl_{24}$). The intersection of the two linear regions provides the CAC.

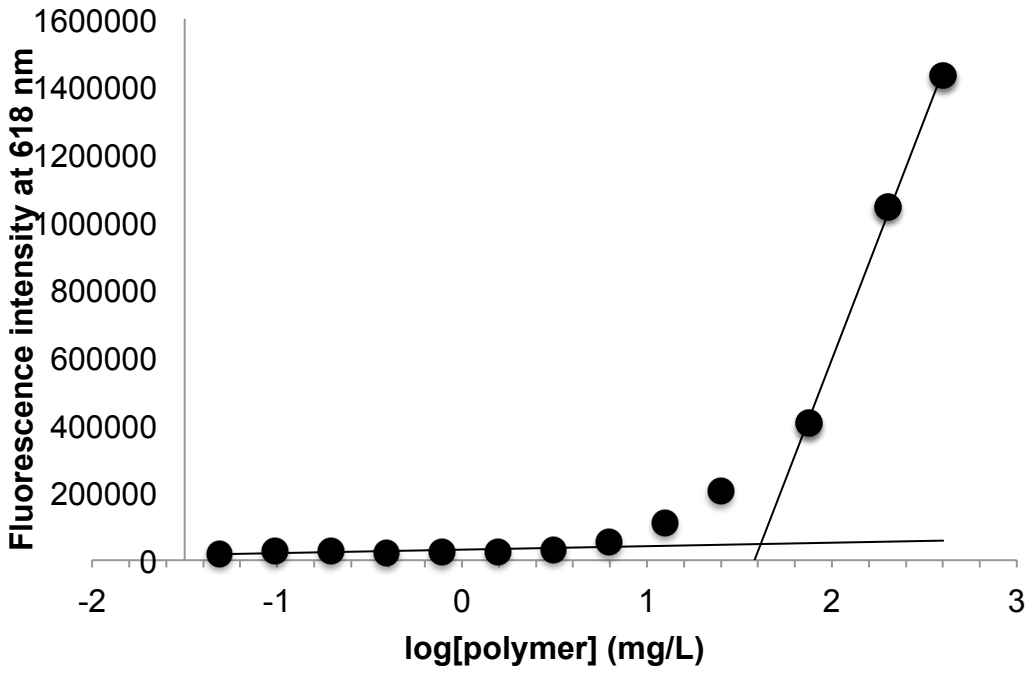

Figure S48. Fluorescence intensity of nile red versus log(concentration of PEO_{45}-*b*-$PHEL_{31}$-TEG_{14}). The intersection of the two linear regions provides the CAC.

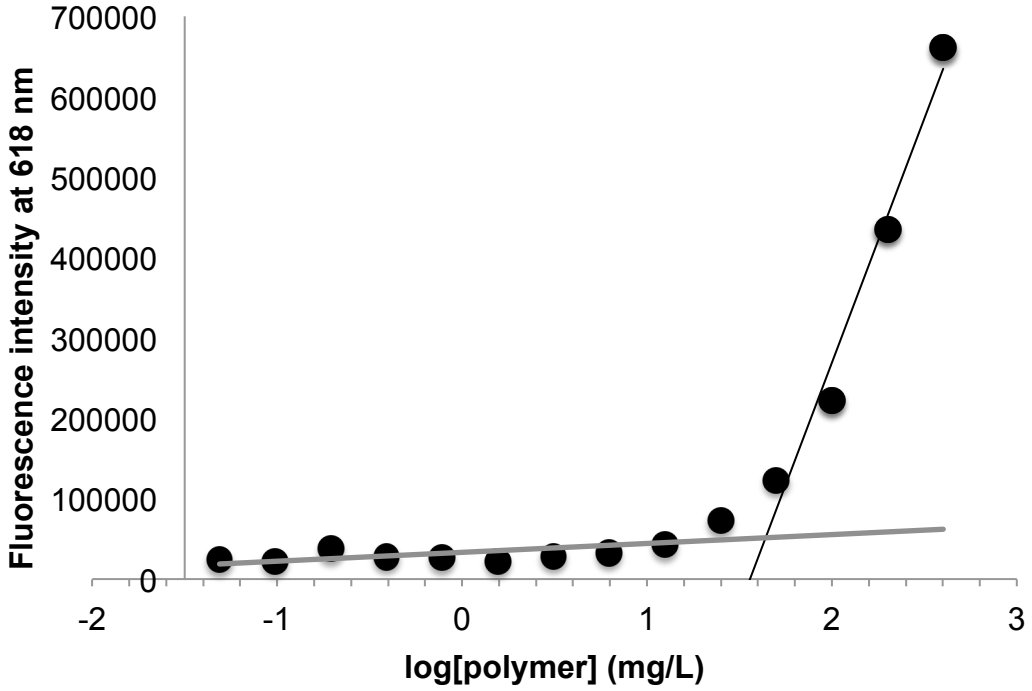

Figure S49. Fluorescence intensity of nile red versus log(concentration of PEO_{45}-*b*-$PHEL_{20}$-CA_{25}). The intersection of the two linear regions provides the CAC.

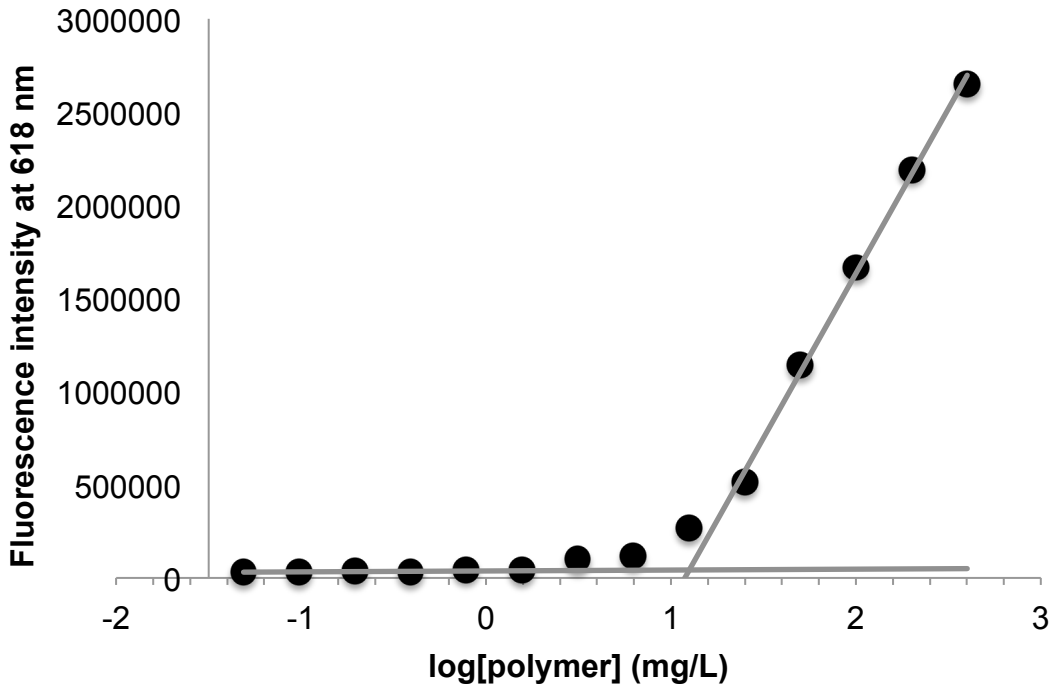

Figure S50. Fluorescence intensity of nile red versus log(concentration of PEO_{45}-*b*-$PHEL_{20}$-CA_7-PTX_{18}). The intersection of the two linear regions provides the CAC.

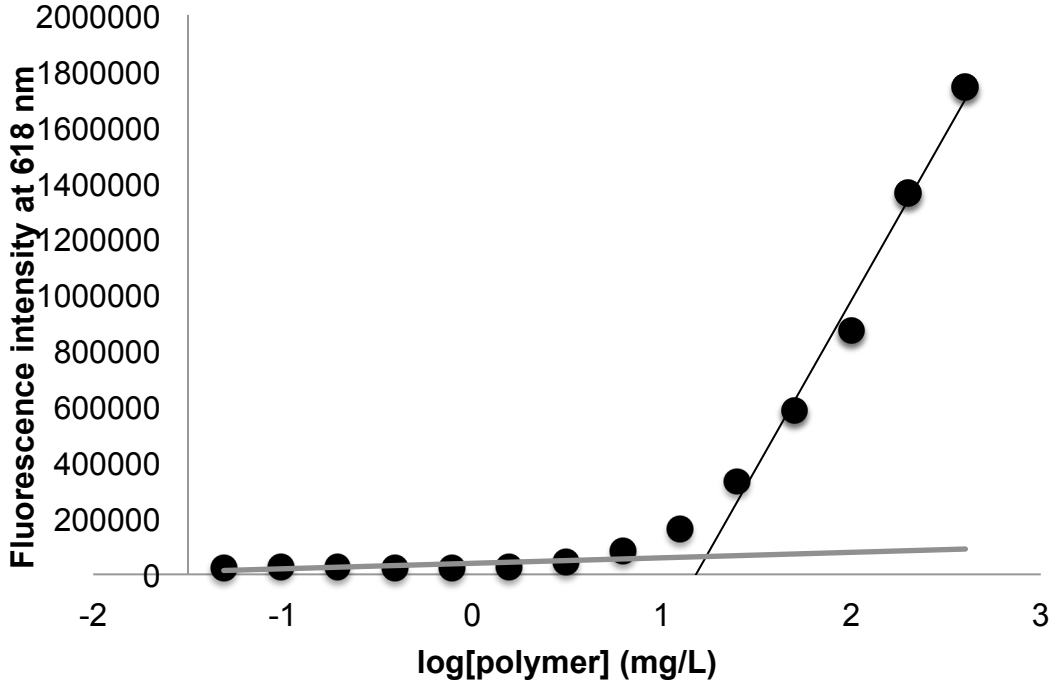

Figure S51. Fluorescence intensity of nile red versus log(concentration of PEO_{45}-*b*-$PHEL_{40}$-RHD_5). The intersection of the two linear regions provides the CAC.

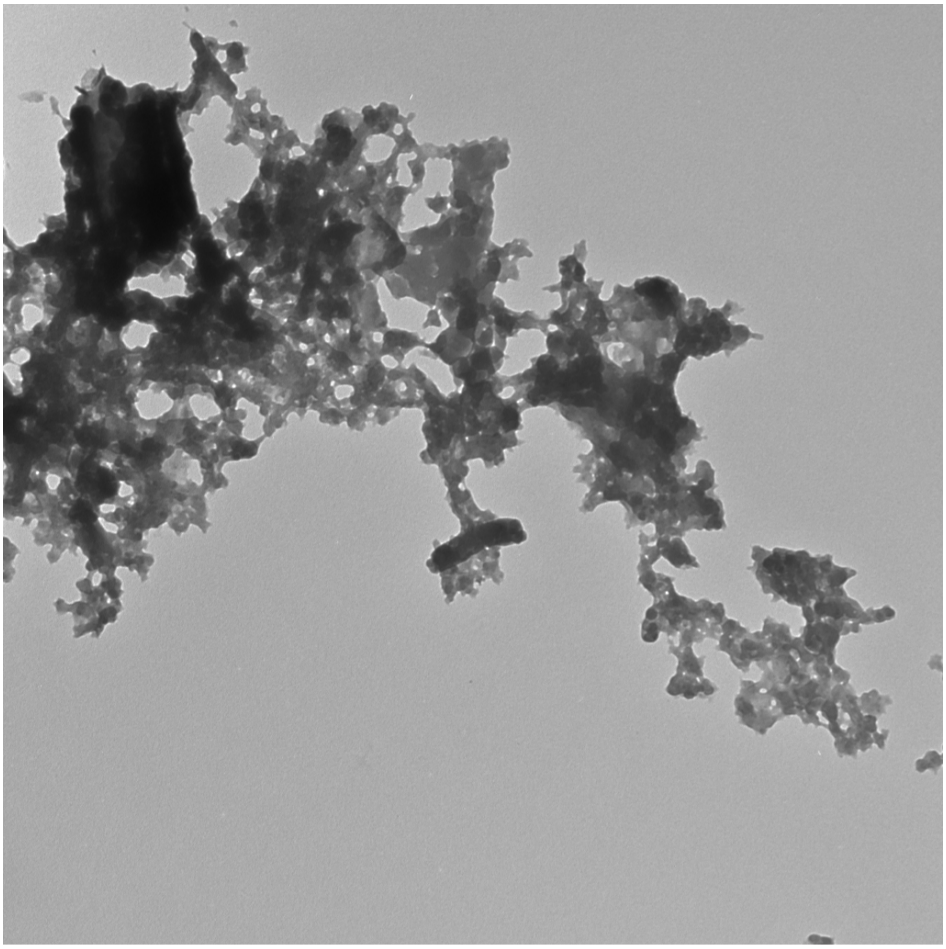

Figure S52. TEM image of assemblies formed from PEO_{45}-*b*-$PHEL_{20}$-CA_7-PTX_{18} upon solvent exchange from THF/water.

References

1. X. Zhang, Y. Shiraishi and T. Hirai, *Org. Lett.*, 2007, **9**, 5039-5042.